Master's thesis

NTNU
Norwegian University of Science and Technology
Faculty of Engineering
Department of Energy and Process Engineering

Lars Martin Ingebrigtsen

Effects of Ultrasonic Frequency, Acoustic Power, and Liquid Height on Radical Production in a Sonochemical Reactor

Master's thesis in Energy and Environmental Engineering
Supervisor: Professor Bruno G. Pollet
June 2019

NTNU
Norwegian University of
Science and Technology

Lars Martin Ingebrigtsen

Effects of Ultrasonic Frequency, Acoustic Power, and Liquid Height on Radical Production in a Sonochemical Reactor

Master's thesis in Energy and Environmental Engineering
Supervisor: Professor Bruno G. Pollet
June 2019

Norwegian University of Science and Technology
Faculty of Engineering
Department of Energy and Process Engineering

NTNU
Norwegian University of
Science and Technology

Sammendrag

Vannelektrolyse, kombinert med høyintensitets ultralyd, har vist potensial til å forbedre hydrogenproduksjon. Imidlertid er det nødvendig med videre forskning innen sonokjemi for å bestemme hvordan forskjellige parametere påvirker sonokjemisk aktivitet. I denne masteroppgaven er eksperimenter blitt gjort for å avdekke hvordan ultralydfrekvens, akustisk effekt og væskehøyde påvirker produksjonen av radikaler. Relevant teori og litteratur er også presentert. Akustisk effekt ble bestemt av kalorimetri for hvert eksperimentelt oppsett. Frekvenser på 24, 580, 860 og 1140 kHz ble studert ved fem forskjellige amplituder (20, 40, 60, 80, 100%) og væskehøyder (85,7, 121,5, 148,6, 185,1, 222,0 mm) ved bruk av en sonokjemisk reaktor med avkjøling. Både en horntransduser (24 kHz) og en platetransduser (580, 860, 1140 kHz) ble brukt. For å bestemme effekten av frekvens og akustisk effekt ble væsken mettet med argon. Produksjon av radikaler ble bestemt ved både Weissler og Fricke dosimetri, med maksimale absorpsjonsbølgelengder på henholdsvis 350 og 304 nm. Optimale væskehøyder ble sett hovedsakelig ved 85,7 mm, men også ved 185,1 mm. Videre hadde 580 og 860 kHz tilsvarende sonokjemiske effektiviteter, som var høyere enn de observert ved 24 og 1140 kHz. I tillegg ble det observert økt kjemisk aktivitet ved en økning i akustisk effekt.

Abstract

Water electrolysis, coupled with power ultrasound, has shown the potential to enhance renewable hydrogen production. However, further research in sonochemistry is needed to determine the effects of different parameters on sonochemical activity. In this thesis, the effects of ultrasonic frequency, acoustic power, and liquid height on radical production have been investigated. Relevant theory and literature are also presented. The acoustic power was determined by calorimetry for each experimental setup. Frequencies of 24, 580, 860, and 1140 kHz where studied at five different amplitudes (20, 40, 60, 80, 100%) and liquid heights (85.7, 121.5, 148.6, 185.1, 222.0 mm) using a sonochemical reactor with cooling. Both a horn-type transducer (24 kHz) and plate transducer (580, 860, 1140 kHz) were used. For determining the effect of frequency and acoustic power, the liquid was saturated with argon gas. Radical production was determined by both Weissler and Fricke dosimetry, at maximum absorption wavelengths of 350 and 304 nm, respectively. The optimal liquid heights were seen mostly at 85.7 mm but also at 185.1 mm. Moreover, 580 and 860 kHz had similar sonochemical efficiencies, which were higher than those at 24 and 1140 kHz. Additionally, the sonochemical activity increased as acoustic power was increased.

Preface

This thesis is a continuation of the work done in TEP4550 - Specialization Project [1] and is part of the course TEP4900 - Master's Thesis. The work concluded my Master's Thesis in Energy and Environmental Engineering and was done during the spring semester of 2019, at the Department of Energy and Process Engineering (EPT) at Norwegian University of Science and Technology (NTNU).

First and foremost, I would like to express my gratitude to Professor Bruno G. Pollet who as my supervisor, has given me guidance and inspiration on how sonochemistry possibly can enhance sustainable hydrogen production in the future. Furthermore, I would like to thank Ph.D. Candidate Md Hujjatul Islam for the time he has spent helping me in the laboratory, providing both helpful advice and necessary equipment for my research. Finally, I would like to thank Raúl Erades de Quevedo, Poul Geffroy, and Antoine LeBoulder for assistance during the semester.

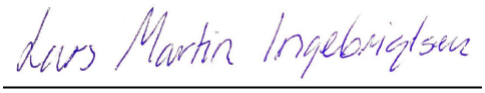

Trondheim, June 22, 2019

List of Figures

List of Tables

Contents

1 Introduction

As the world faces over-exploitation of finite natural resources and fossil fuels, concurrent with increasing energy demands, more sustainable solutions are imperative. Energy plays a vital role not only in the extraction of natural resources but in most industrial sectors and our everyday life. Hereupon, it is crucial to develop technological solutions to ensure efficient renewable energy production and storage. Such actions can be a remedy and result in a decline in the use of fossil fuels like coal, oil, and natural gas [2], [3].

Hydrogen is currently considered as one of the most promising energy carriers for the future, partially due to its high specific energy compared to other fuel types. Already in 1874, Jules Verne predicted that *"water will be the coal of the future"*. Not long after in the 1930s, the German engineer Rudolf Errand spoke about how hydrogen from water electrolysis could be used as fuel for transportation [3]. Nonetheless, today about 90% of the hydrogen originates via oil and natural gas reforming with efficiencies from 70-100%. Despite high efficiencies, the production generates vast amounts of greenhouse gases such as CO_2 [2].

Other methods for hydrogen production include ethanol gasification, biological photosynthesis, photocatalysis and water electrolysis. The latter currently accounts for about 4% of the entire hydrogen production, with an efficiency of 56-73% for commercially available electrolysers. Despite a low efficiency compared to the ones observed for oil and natural gas reforming, water electrolysis coupled with power ultrasound shows promise to enhance sustainable hydrogen production [2], [4].

Power ultrasound refers to sound above 20 kHz at high powers, and when applied to water, acoustic cavitation occurs. The cavitation bubbles collapse very violently, splitting the water molecules inside and at the vicinity of the bubble. Subsequently, hydrogen gas (H_2), hydroxyl radicals ($OH\cdot$), hydrogen peroxide (H_2O_2) and other chemical species form. Moreover, in a sonoelectrochemical cell, power ultrasound enhances mass transfer, activates the surface of the electrode and removes gas bubbles. Whereas only some studies have investigated how these sonoelectrochemical processes behave, more research is needed in sonochemistry to unravel the phenomena of acoustic cavitation further [2], [5].

In the relatively new field of sonochemistry, the effect of ultrasound on chemical reactions is studied. An ultrasonic transducer, in combination with a sonoreactor or ultrasonic bath, is usually employed for studying sonochemical activity. However, many parameters affecting the sonochemical reactions, such as power, frequency, temperature, geometry, and dissolved gas, are not fully understood. By investigating a sonochemical setup under different conditions, it can be characterised, and possibly help in the identification of optimal parameters for sonochemical activity [2], [6].

Being that acoustic cavitation bubbles have a very short lifespan and the radicals produced recombine quickly, it is challenging to determine the sonochemical activity. The $OH\cdot$ species is considered the most interesting in relation to acoustic cavitation due to its dominant role in a collapsing bubble. A solution for determining the sonochemical activity is to add a chemical dosimeter to the water, which traps the radicals before they react with other species. Several different chemical dosimetry methods exist, some being more favorable than others when it comes to reliability, cost, and simplicity [2].

2 Theory and Literature Review

In the following subsections, the theory and literature review for this thesis are found. As mentioned, this thesis is a continuation of the work done in TEP4550 - Specialization Project [1], and as such, there is some reproduction and usage of the content therefrom. Section 2.1 presents the definition and requirements of power ultrasound, while Section 2.2 explains the physics and observations regarding the phenomenon of acoustic cavitation. Further, Section 2.3 and 2.4 clarify the mechanisms behind producing ultrasound and categorises different varieties of sonochemical setups. As for Section 2.5, the chemistry germane to acoustic cavitation bubbles is summarised, with additional subsections about the use of calorimetry in sonochemistry and the effect of different parameters. Finally, in Section 2.6 and 2.7 different dosimeters and characterisation tools is elucidated.

2.1 Power Ultrasound

Ultrasound refers to sound waves above the human hearing range, i.e., above 20 kHz. It is applied in medical imaging, cleaning, and chemical processing among others. The lower spectrum between 20 kHz and 100 kHz is defined as power ultrasound or low frequency ultrasound. The power ultrasound range can in some cases be extended up to 2 MHz. In other areas of use, including medical diagnostics and acoustic microscopy, ultrasound frequencies reach up to 10 MHz and several gigahertz, respectively [5]. Although the sound is above the human hearing range, some audible sound with frequency below 20 kHz can be radiated into the atmosphere during experiments due to nonlinear effects [6].

Also, in order to have power ultrasound, the acoustic intensity (I) has to exceed the threshold intensity for which a violent bubble collapse can occur. The acoustic intensity is defined as *"the energy flow through an unit area normal to the wave propagation direction"* [6]. The threshold intensity corresponds to a specific pressure amplitude (p_a), which both become greater at higher frequencies. The pressure amplitude is the maximum increase or decrease in pressure due to the the displacement amplitude from the propagating wave. Both the threshold for pressure amplitude and intensity for some frequencies are shown in Table 2.1. These values only applies for travelling waves in water, made from a planar source (plane waves) or point source (spherical waves). Although the threshold is the same for standing and travelling waves for pressure amplitude, the intensity threshold may be different [6].

Table 2.1: Acoustic intensity and acoustic pressure amplitude threshold for some frequencies [6]

Frequency	$I_{threshold}$	$p_{a,threshold}$
20 kHz	0.49 W/cm^2	1.2 atm
140 kHz	0.88 W/cm^2	1.6 atm
1 MHz	3 W/cm^2	3 atm
5 MHz	11 W/cm^2	5.8 atm

Power ultrasound can be used in mainly two different ways. Either to induce mechanical vibration on the surface of a solid directly from the transducer, or indirectly induce acoustic vibration causing cavitation in a fluid. In relation to sonochemistry and the production of hydrogen, the indirect method is the one that is relevant [5].

2.2 Acoustic Cavitation

The induced acoustic vibration by power ultrasound causes the formation and subsequent collapse of cavitation bubbles. This is explained by how ultrasound is propagated through a medium as compression and rarefaction waves. With sufficient ultrasound intensity, attractive molecular forces are exceeded (in the rarefaction cycle). In this phase, the amplitude pressure becomes larger than the ambient pressure (normally at 1 atm). This results in a negative pressure which forces the liquid to expand, creating cavitation bubbles. For each compression and rarefaction cycle, the bubble grows, until the bubble reaches an unstable size and implodes during the compression phase of the cycle. Such a implosion is called acoustic cavitation [5]. Also, acoustic cavitation is not to be confused with boiling. While the origin of bubble formation is due to a pressure reduction during acoustic cavitation, boiling is due to heating. Furthermore, there is no presence of violent bubble collapse in boiling [6]. In Figure 2.1, the growth process of a cavitation bubble is illustrated.

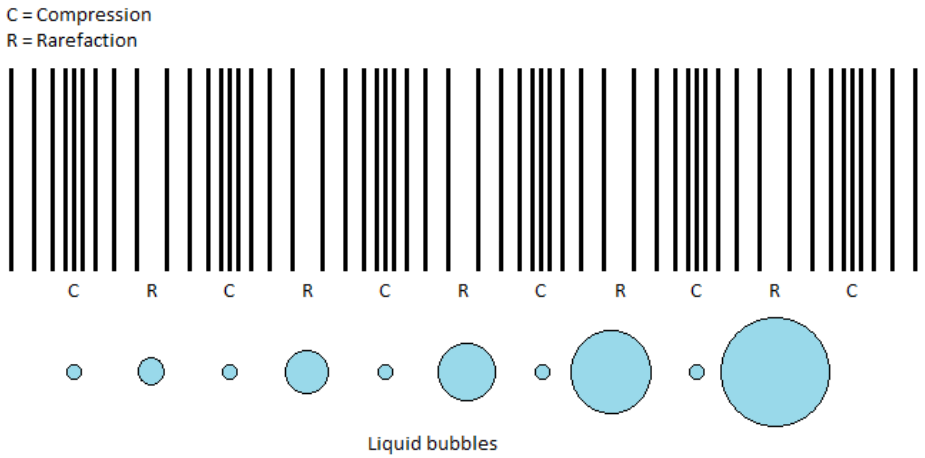

Figure 2.1: The compression and rarefaction cycle of a longitudinal sound wave, compared to the growth of a cavitation bubble.

In a multi-bubble aqueous system, local pressure and temperature rise abruptly up to as high as 2000 atm and 5000 K, and can be perceived as a microreactor during acoustic cavitation. Furthermore, temperature has been shown to be dependent on the solution, and can be even higher for single-bubble systems [7]. The implosive collapse has a lifespan of less than 100 ns. In addition, collision densities of 1.5 kg/cm^2, pressure gradients of 2 TPa/cm, and cooling rates of 10^{10} K/s can be seen [5]. The maximum theoretical bubble temperature (T_{max}) and the theoretical maximum bubble pressure (P_{max}) can be calculated by equation 2.1 and 2.2, respectively.

$$T_{max} = T_0\left(\frac{P_m(\gamma - 1}{P_v}\right), \tag{2.1}$$

$$P_{max} = P_v\left(\frac{P_m(\gamma - 1}{P_v}\right)^{\frac{\gamma}{\gamma-1}}. \tag{2.2}$$

For these equations, T_0 is the temperature of the ambient solution, P_m is the sum of the hydrostatic and acoustic pressure, P_v is the bubble pressure at maximum size, and $\gamma = c_p/c_v$ is the specific heat ratio of the gas/vapour inside the bubble [8].

In the near vicinity of an extended surface, the cavity collapse can only occur asymmetrically and becomes non-spherical. This creates a high-speed jet towards the solid surface of up to 200 m/s [9]. This violent jet is associated with what is known as cavitation corrosion and can cause significant damage to a solid wall [10].

Two types of cavitation bubbles could be generated during sonication. These are called transient (or inertial) and stable (or non-inertial) cavitation bubbles. The stable cavitation bubble is actually repetitive transient, meaning that it nearly collapses and grows several times. This repetition can in some cases go on for several days. The transient cavitation bubble has a much shorter lifespan and collapses only after a few acoustic cycles [7], [8], [11]. Stable and transient cavitation can also be defined in a different manner. Transient cavitation occurs with sonochemical reactions and sonoluminescence (light emission), while stable cavitation does not. Depending upon the definition used, some bubbles can be both transient and stable, meaning that the bubble can have a long lifetime with accompanying sonoluminescence and chemical reactions. The light emitted from such bubbles can be seen with the naked eye [6].

2.3 Ultrasonic Transducers

The ultrasonic transducers exploit the inverse piezoelectric effect to produce ultrasonic waves, which is the same effect that is utilised in speakers. This effect describes the deformation of a material by applying an electric field. In an opposing manner, piezoelectricity occurs only in certain solid materials (called *piezoelectric materials*) that produce electricity due to the latent heat or pressure. Such materials also have the inverse piezoelectric effect, and in ultrasonic transducers, common materials for this purpose are barium titanate ($BaTiO_3$), lead zirconate titanate (PZT), and crystallized quartz (SiO_2). As voltage is applied to a piezoelectric material, its molecules become negatively and positively charged. This results in an attractive force between these ions, which causes a slight deformation in the material. The application of AC voltage causes the material to compress and expand with the same frequency as the AC voltage. Figure 2.2 illustrates this alternating deformation. The strongest vibrations occur at the vibration corresponding to the resonance frequency of the piezoelectric material and are determined by its stiffness and mass [6].

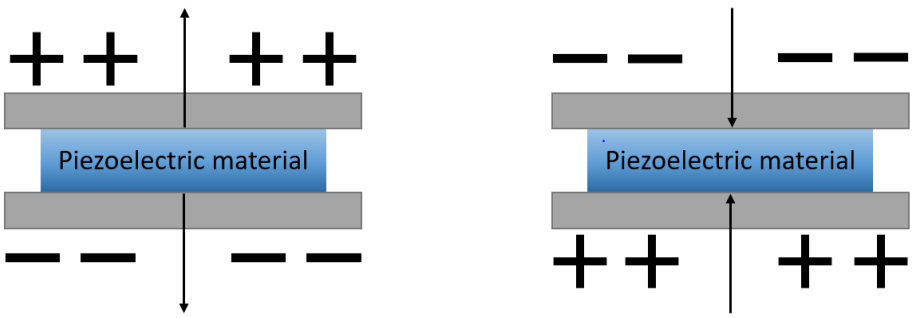

Figure 2.2: Alternating deformation caused by the inverse piezoelectric effect. The parts with gray colour is metal plates which are connected to a voltage source.

Two types of configurations are used for ultrasonic irradiation, dependent upon frequency. For lower frequencies in the range 20-200 kHz, the bolt-clamped Langevin-type transducer (BLT) is used. The BLT is made up of a piezoelectric ceramic which is firmly pressed between two metal plates. The metal plates cause the resonance frequency to decrease, which reveals why the BLT is more preferred for lower frequencies. For high frequencies in the range 100 kHz to 1 MHz, a thin piezoelectric plate is used with an accompanying vibration plate [6].

Although a BLT produces lower frequencies, the acoustic intensity (I) is often considered too low for ultrasonic irradiation of liquids. The acoustic intensity describes the energy flux normal to the wave propagation direction, as mentioned in Section 2.1. Measurable in $\mathrm{W/m^2}$, it is mathematically defined by equation 2.3:

$$I = \frac{p_a^2}{2 \cdot \rho_0 \cdot c}, \tag{2.3}$$

where p_a is the acoustic pressure amplitude for a plane or spherical sinusoidal wave, ρ_0 is the density of the liquid, and c is the speed of the sound wave. As seen from this equation, the intensity increases with an increase in acoustic pressure amplitude. Considering that the acoustic pressure amplitude decreases with growing surface area, it is preferable to have a small surface area to achieve high intensity. Thus, a horn-type transducer is usually favored rather than the BLT. The horn-type transducers are made by coupling the BLT with an integer number of half-wavelength (equivalent to the half-wavelength of the acoustic wave at resonance frequency) metal plates [6].

2.4 Ultrasonic Reactors and Baths

Sonoreactors come in many different forms, shapes, and sizes, which are mainly dependent on their purpose. Primarily, sonochemical configurations are divided into two categories. First, there are the ultrasonic baths with one or several ultrasonic transducers placed in the periphery of the reaction vessel, and second is where the ultrasonic sonotrode typically is immersed into the liquid [5]. A simple configuration of these is illustrated in Figure 2.3.

Normally, the ultrasonic bath is made of stainless steel and used for cleaning purposes [8]. Both direct and indirect irradiation is possible, meaning that when indirect sonication occurs, a smaller liquid container is immersed in the bath [5]. For the ultrasound to penetrate the reaction vessel during indirect sonication, the thickness of its sole plate should be taken into consideration. Sufficient thinness should either be less than 1/10 of the ultrasonic wavelength, or an integer multiple of the half wavelengths [12]. For laboratory use, the size of the ultrasonic baths can range from less than 1 L to tens of litres.

For the horn-type sonoreactors, reaction vessels range from simple beakers to advanced sonochemical apparatus. The liquid can either be stationary or flow through the reactor. As for the stationary ones, a water circulation cooling system is often present [8]. Other configurations can include a pressure system and attachments for gas connections and measuring equipment. Both glass and steel reactors exist.

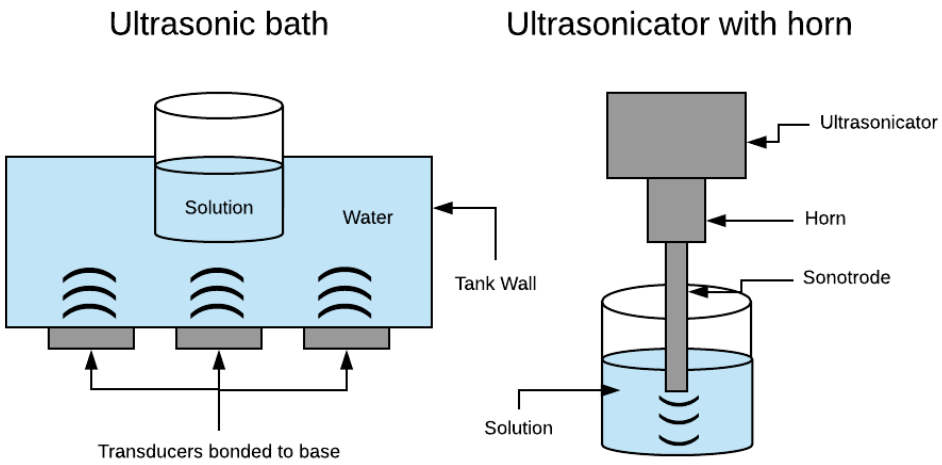

Figure 2.3: Illustration of an ultrasonic bath and an ultrasonicator with the sonotrode immersed in water. For the ultrasonic bath, the water and solution are exposed to direct and indirect sonication, respectively.

Although ultrasonic baths often operate at high power, the majority of sonochemical activity reported is carried out by using the horn-type transducer in direct contact with the liquid. Such systems provide acoustic energy with higher intensity due to the magnification of mechanical vibrations through the sonotrode [8]. Sonochemical activity is elucidated further in the following Section 2.5.

2.5 Sonochemistry

The study of sonochemistry is relatively new and is concerned about how ultrasound can affect chemical reactions. Ultrasonication of aqueous solutions causes sonochemical reactions and processes due to the phenomenon of acoustic cavitation as described in Section 2.2. The effects are both chemical and mechanical and occur inside the collapsing bubble (transient bubbles) and in its vicinity. The stable bubbles have a less violent collapse and do not contribute to sonochemical reactions. The cavity collapse is divided into single- or multi-bubble collapse, where the latter is dominant [13].

Both homogeneous (same phase) and heterogeneous (different phase) reactions take place during acoustic cavitation. The cavitation bubbles consist of a mixture of water vapour as well as other gas species, depending on the solution. As bubble implosion takes place and extreme temperature and pressure conditions occur, the water vapour, and other dissolved gases undergo fragmentation. Hence, radicals such as $H\cdot$ $OH\cdot$, $HO_2\cdot$, and other species like H_2O_2, O, and O_3, are formed [2].

Although many sonochemical reactions occur during acoustic cavitation in water, the production of hydroxyl radicals ($OH\cdot$) is the most interesting in relation to sonochemical activity. Compared to other products like O, O_3 and H_2O_2, the $OH\cdot$ radicals are also the most dominant product [2]. However, the role of O atoms is still unclear but is assumed to react with the liquid water at the bubble vicinity [6]. Like the other reactive species mentioned, the $OH\cdot$ radicals are produced by the splitting of the water molecule, as shown in reaction 2.4.

$$H_2O \longrightarrow H\cdot + OH\cdot \tag{2.4}$$

The oxidation-reduction potential of some common oxidants is shown in Table 2.2.

Table 2.2: Oxidation-reduction potential of some common oxidants [6].

Reaction	Potential [V]
$O\cdot + 2\,H^+ + 2\,e^- \longrightarrow H_2O$	2.421
$O_3 + 2\,H^+ + 2\,e^- \longrightarrow O_2 + H_2O$	2.076
$OH\cdot + e^- \longrightarrow OH^-$	2.02
$H_2O_2 + 2\,H^+ + 2\,e^- \longrightarrow 2\,H_2O$	1.776
$HO_2 + H^+ + e^- \longrightarrow H_2O_2$	1.495

During the short lifetime of the $H\cdot$ and $OH\cdot$, the radicals form molecular hydrogen by the gas phase recombination reaction (2.5), and the recombination reaction at the shell (reaction 2.6) inside the bubble and at the wall, respectively. However, it has been shown through numerical simulations that reaction 2.5 is responsible for more than 99.9% of molecular hydrogen production [4], [14].

$$H\cdot + OH\cdot \longrightarrow H_2 + O \tag{2.5}$$

$$H\cdot + H\cdot \longrightarrow H_2 \tag{2.6}$$

In addition, about 20% of the $OH\cdot$ can diffuse to the bubble surface where temperatures are lower, and form H_2O_2 (reaction 2.7) [15].

$$OH\cdot + OH\cdot \longrightarrow H_2O_2 \tag{2.7}$$

2.5.1 Calorimetry for Sonochemistry

In sonochemistry, the acoustic power describes the ultrasonic energy that is dissipated in the liquid during sonication. In order to determine the acoustic power for a sonochemical setup, standard calorimetry is usually used. Such a method is based on measuring the temperature rise in a reaction cell during sonication, starting at thermal equilibrium with the surroundings. In order to avoid heat transfer to the surroundings during sonication, the reaction vessel should be insulated as much as possible. If the vessel walls consist of a highly conductive material, with high heat capacity, the change in heat content may also be considered [16]. By determining the acoustic power one is able to calculate the sonication efficiency or yield for the experiments performed. This is essential for comparison with other reported results. The ultrasonic power dissipated into the liquid can be obtained by the following equation [17]:

$$P = c_p \rho V \left(\frac{dT}{dt}\right)_{t=0}. \tag{2.8}$$

Here, c_p is the heat capacity of the liquid, ρ is the density of the liquid, V is the volume of the liquid, and $(dT/dt)_{t=0}$ is the initial rate of the temperature change. A measuring period of about one minute can be used in order to determine the initial

rate of temperature change. With such a small measuring period, it is essential to have responsive and accurate thermocouples. The thermocouples should also preferably be placed in the middle of the liquid, and not directly under the sonotrode as the sonication may cause interference. As the temperature change during measurements is relatively small, both c_p and ρ is considered to remain constant [1].

Measurements should be repeated several times in order to get good results. By plotting each run with a curve fitting line of 2^{nd} order polynomial, the curve fitting equations can be differentiated and evaluated in t = 0. In such a way, $(dT/dt)_{t=0}$ is obtained [1].

2.5.2 Effect of Acoustic Intensity

The acoustic intensity is closely related to the acoustic power as described in the previous section. As mentioned in Section 2.1, a certain amount of acoustic intensity (frequency dependent) is required to achieve acoustic cavitation. This part focuses on acoustic intensities beyond this threshold.

The radical production inside a collapsing bubble is mainly determined by three factors, bubble temperature, bubble collapse time, and amount of water vapour trapped in the bubble. As ultrasonic intensity increases, the bubble expansion and compression ratio increase. The increased compression ratio causes bubble temperatures to rise, while an increased expansion ratio enables the bubble to trap more vapour. Moreover, the bubble collapse time is increased due to increased acoustic intensity, giving more time for chemical reactions to occur inside the bubble. Hence, all three effects of increased intensity promote radical yield [2].

Also, Ashokkumar and Mason [8] report that an increase in the number of active cavitation bubbles and the bubble size can be expected with an increase in acoustic power and intensity. They refer to the rise in bubble temperature as the cause of increased bubble size. At higher frequencies, the increase in the H_2 production was more noticeable as acoustic intensity was increased than for lower frequencies [4]. Wood et al. [18] state that when the acoustic pressure amplitude is high (related to acoustic intensity by equation 2.3), the bubble surface oscillations and the non-linear bubble can result in bubble separation. Hence, new bubbles contributing to sonochemical activity are formed.

2.5.3 Effect of Ultrasonic Frequency

Frequency has many effects on the sonochemistry occurring in an irradiated liquid, and according to Islam et al. [2] it is the dominant factor that affects sonochemical activity. As mentioned in Section 2.2, frequency affects the ratio between transient and stable bubbles formed. It also affects the number of bubbles, their size, and distribution throughout the liquid. Although many other factors like temperature and geometry affect these cavitation properties, higher frequency tends to produce a greater amount of bubbles with a smaller size than for lower frequencies. This can be explained by the increased rate of oscillation for higher frequencies, which causes the smaller bubbles to reach their resonance size more efficiently. The ultrasonic frequency is inversely related to a bubbles resonance size. On the other hand, more power is required for cavitation to occur at a higher frequency due to an increased cavitation threshold [8], [18].

The number of bubbles, as well as the size of the bubbles, is shown to be among other factors frequency dependent. The size of the bubbles increases with lower frequencies.

Cavitation bubbles at a sonication frequency of 20 kHz have been measured to have a theoretical resonance radius of 150 µm, while for 1056 kHz this radius is 3 µm. The larger bubbles contain more water vapour, resulting in higher generation of primary radicals at lower frequencies. In spite of this, the maximum radical yield is considered to be in the range of 200-600 kHz, due to the total number of bubbles [7]. However, most sonochemical experiments are performed at 20 kHz [2].

Through the multi-bubble sonoluminescence (MBSL) quenching technique which takes into account multi-bubble processes such as rectified diffusion and bubble coalescence, it has been shown that the bubble type is dependent on frequency, with a transition from transient bubbles to stable bubbles at 200 kHz [19].

2.5.4 Effect of Bulk Liquid Temperature

With increased bulk liquid temperature, the cavitation threshold decreases. This is due to the reduced surface tension and viscosity in the liquid. As temperature rises, the vapour pressure increases and leads to a greater molecular transitioning of vapour into the bubble. Although an increased amount of vapour inside a bubble can enhance the sonochemical activity, the increased liquid temperature causes a damping effect. This occurs due to a reduction in γ which reduces the temperatures during a bubble collapse [4]. Varying temperature also has an effect on H_2O_2 yield and can shift the maximum production from one frequency to another [18].

Furthermore, due to liquid properties, the gas solubility decreases with increased temperature, causing fewer cavitation nuclei in the liquid [18]. It is reported [4] that there is an optimum temperature of approximately 30 °C for sonochemical production of H_2 production in an argon saturated solution. Further, the bulk liquid temperature has shown not to affect the expansion and compression ratio [4].

2.5.5 Effect of Geometry

It has been reported [20], [21] that slight changes in the geometry of a sonoreactor resulted in noticeable changes to the sonochemical reactions occurring during sonication. With different geometries, different acoustic fields are generated. It has also been pointed out that there is very limited knowledge about lab-scale sonoreactors, making it challenging to develop efficient industrial-scale sonoreactors [22], [23].

Some researchers studied the effect of ultrasound irradiation distance on the sonochemical activity at 36 and 108 kHz. By using a cylindrical glass reaction vessel with liquid levels from 8-34 cm, they showed that the cavitation yield increased considerably with increasing liquid levels [24].

Additionally, Contamine et al. [17] studied the effect of volume and liquid height for a cylindrical vessel of 5 cm in diameter. With this geometry, they tested the liquid heights of 2.8, 3.9, and 5.3 cm and found that the specific acoustic energy (acoustic energy divided by volume) was almost independent on liquid height.

2.5.6 Effect of Dissolved Gases

Monoatomic gases usually have a higher polytropic ratio ($\gamma = C_p/C_v$) than polyatomic gases. In addition, gases with low thermal conductivities (k), reduce the heat dissipation.

Both these properties promote sonochemical activity due to increased temperature during bubble collapse. This is also seen from equation 2.1. The overall sonochemical activity is also affected by the number of transient bubbles as well as the size of the bubble. It is found that the number of active bubbles is proportional to the solubility (S_g) of the gas. Highly soluble gases also lower the threshold for nucleation, likely caused by reduced surface tension in the liquid. Thus, a higher solubility gives more overall sonochemical activity [2]. Polytropic ratio, thermal conductivity, and solubility at 20°C and 1 atm for some typical gases are listed in Table 2.3.

Table 2.3: Polytropic ratio, thermal conductivity, and solubility (grams of dissolved gas per liter water) for some typical gases [25], [26], [27].

Gas	Polytropic Ratio (γ)	Thermal Conductivity (k)	Solubility (S_g)
Argon	1.66	0.016 W/m^{2}K	0.062 g/L
Air	1.41	0.026 W/m^{2}K	0.021 g/L
CO_2	1.28	0.015 W/m^{2}K	1.69 g/L
CO	1.40	0.023 W/m^{2}K	0.028 g/L
Hydrogen	1.41	0.168 W/m^{2}K	0.0016 g/L
Nitrogen	1.40	0.024 W/m^{2}K	0.019 g/L
Oxygen	1.40	0.024 W/m^{2}K	0.043 g/L

Argon is often used in sonochemistry to enhance sonochemical activity. This is due to its high polytropic index, low thermal conductivity, and high solubility, but also because the gas is relatively inexpensive. The effect of argon on sonochemical activity is dependent upon frequency [18].

Oxygen saturation causes several direct effects on sonochemical reactions. During acoustic cavitation the O_2 form the highly reactive $O\cdot$. These radicals recombine with some of the $H\cdot$ resulting in less production of H_2O_2. The effect of oxygen saturation is also frequency dependent. At low frequencies less $H\cdot$ diffuse to the vicinity of the bubble, and some of the O_2 may form the hydroperoxyl radical by reaction 2.9 [18].

$$H\cdot + O_2 \longrightarrow OOH\cdot \tag{2.9}$$

For CO_2 saturation, active cavitation is inhibited because of its acidic nature when dissolved. Upon dissolution, a greater number of stable bubbles is seen, resulting in less radical production. With the high solubility for CO_2 in water seen in Table 2.3, more CO_2 diffusion occurs into the bubble during acoustic cavitation. This results in a cushioning effect during bubble collapse, due to a reduction in heat as well as disassociation inside the bubble. In addition, the dissolved CO_2 lowers the pH of the solution, which causes an increase in the diffusion of charged species to the bubble surface. This increase in surface charge reduces bubble coalescence and influences the adsorption between vapour and liquid at the surface [18].

Although argon saturation increases the radical yield significantly, a gas mixture of 80% argon and 20% oxygen have been shown to be even more efficient for the H_2O_2 production. This will vary with experimental setup and ultrasonic frequency. Furthermore, small amount of He, O_2, N_2 and even CO_2 has shown to increase sonochemical rates. For the oxidation of I^-, these rates decrease significantly with more than 3% CO_2 [18].

2.6 Dosimetry Methods

Measuring the formation of radicals in an aqueous solution during sonication is challenging due to the radical's short lifespan. By introducing other soluble chemicals in the water that scavenge the highly reactive $OH\cdot$ or H_2O_2, one can quantitatively determine the produced amount of such species after sonication. Such measuring techniques are called aqueous chemical dosimetry methods.

Several chemical dosimeters for determining the hydrogen peroxide or hydroxyl radical formation during ultrasonication are presented below. While methods such as terephthalic acid dosimetry offer high sensitivity, Fricke and Weissler dosimetry are considered reliable, but not sensitive enough when very high accuracy is needed. Scalability applies to all the methods mentioned in terms of volume.

To represent the energy-specific yield for a dosimeter, the G or sonochemical efficiency (SE) value can be obtained [16], [28]. Measurable in µmol/kJ, they represent the total amount of molecules produced per energy unit. The SE can be used based on any chemical species and can be obtained from the following equation:

$$SE = \frac{CV}{Pt}, \tag{2.10}$$

where C [µM] is the concentration, V [L] is the solution volume , P [kW] is the acoustic power, and t [s] is the sonication time.

2.6.1 Weissler Dosimetry

The Weissler (also called *Iodide* or *KI*) dosimetry method was first used by Alfred Weissler [29] who sonicated an aqueous KI solution containing CCl_4, creating a reaction between molecular chlorine and iodide ions to liberate molecular iodine. Due to environmental reasons, CCl_4 is nowadays not in use for this purpose. Instead, the Weissler method is associated with the sonication of pure aqueous potassium iodide (KI) solution. A standard Weissler solution is made by mixing KI and deionized water to a concentration of 0.1 mol/L. There are two reaction pathways essential this dosimetry method [16], [24]. These reaction pathways merge after iodine is produced. The first one is by reaction 2.11 to 2.12, and the second from reaction 2.13 to 2.15.

By reaction 2.11, the $OH\cdot$ produced during sonication come together to form hydrogen peroxide. As mentioned in Section 2.5, this happens for about 20% of the hydroxyl radicals. As seen by reaction 2.12, the hydrogen peroxide reacts with iodide ions and give rise to I_2. As this reaction is slow, a catalyst like molybdate ions can be used to promote reactivity [16].

$$2\,OH\cdot \longrightarrow H_2O_2 \tag{2.11}$$

$$H_2O_2 + 2\,I^- + 2\,H^+ \longrightarrow I_2 + H_2O \tag{2.12}$$

The second reaction pathway is the direct oxidation of iodide ions by the hydroxyl radicals, forming iodine (reaction 2.13). Furthermore, the iodine atoms react with iodide ions to produce $I_2{}^-$ (reaction 2.14), which subsequently give rise to I_2 (reaction 2.15) [16], [28].

$$\mathrm{OH}\cdot + \mathrm{I}^- \longrightarrow \mathrm{OH}^- + \mathrm{I} \tag{2.13}$$

$$\mathrm{I} + \mathrm{I}^- \longrightarrow \mathrm{I_2}^- \tag{2.14}$$

$$2\,\mathrm{I_2}^- \longrightarrow \mathrm{I_2} + 2\,\mathrm{I}^- \tag{2.15}$$

Finally, the molecular iodine (I_2) produced from these two reaction pathways reacts with the excess iodide ions to form triiodide ions ($I_3{}^-$) as seen in reaction 2.16 [16], [28].

$$\mathrm{I_2} + \mathrm{I}^- \longrightarrow \mathrm{I_3}^- \tag{2.16}$$

Additionally, the $H\cdot$ atoms produced during acoustic cavitation will reduce the iodine formed by equation 2.17. Although this is a problem in radiation chemistry, it is often neglected in sonochemistry due to the dominance of $OH\cdot$ compared to $H\cdot$ [6]. As oxygen gas can oxidize the iodide ions under acidic conditions, Iida et al. [16] recommend that the Weissler dosimeter should be used in a limited pH range of 4 to 7, which fortunately is the case when KI is dissolved in deionized water.

$$2\,\mathrm{H}\cdot + \mathrm{I_2} \longrightarrow 2\,\mathrm{I}^- + 2\,\mathrm{H}^+ \tag{2.17}$$

As seen from the reactions above, the formation of a triiodide ion correspond to both one and two hydroxyl radicals, depending upon reaction pathway. The absorbance of $I_3{}^-$ can be measured using a UV-Vis spectrometer. The maximum absorption wavelength has been reported to be 350 nm, 352 nm (ϵ = 26 000 $\mathrm{dm^3mol^{-1}cm^{-1}}$) or 355 nm ($\epsilon$ = 26 300 $\mathrm{dm^3mol^{-1}cm^{-1}}$) [16], [24], [28].

Another variant of the Weissler dosimetry method is also found [30]. Here, purified water is irradiated to form hydrogen peroxide as seen earlier in reaction 2.11. An iodide reagent is made up by mixing 1 mL of two solutions. The first solution consists of 0.4 M of KI, 0.05 M of NaOH, and 0.00016 M of $(NH_4)_6Mo_7O_{24}\cdot 4\,H_2O$, while the second is made up from 0.1 M $KHC_8H_4O_4$. A 1 mL sample from the sonicated solution is then mixed with the iodide reagent, creating a 3 mL solution. By reaction 2.12 and 2.16, triiodide is formed, and measured in the same manner as mentioned above.

2.6.2 Fricke Dosimetry

Fricke dosimetry (also called *ferrous sulfate dosimetry*) is considered one of the most useful dosimeters. Although known, a major disadvantage to the dosimeter is its high sensitivity to impurities that oxidize the ferrous ions or scavenge the hydroxyl radicals [31]. The HO_2 radicals are such a species (see reaction 2.21), which form if oxygen gas is present [16].

A Fricke solution can be prepared by 0.392 g (0.001 mol) of $FeSO_4(NH_4)_2SO_4\cdot 6\,H_2O$, 41.1 g (0.4 mol) of 96% H_2SO_4, and 0.0585 g (0.001 mol) of NaCl dissolved in deionized water, until 1 L solution is obtained. Due to its strong acidity, the solution must be handled with care [32]. During sonication, the hydrogen peroxide and hydroxyl radical oxidize the Fe^{2+} in the solution, as seen in reaction 2.18 and 2.19.

$$\mathrm{OH}\cdot + \mathrm{Fe}^{2+} + \mathrm{H}^+ \longrightarrow \mathrm{H_2O} + \mathrm{Fe}^{3+} \tag{2.18}$$

$$H_2O_2 + Fe^{2+} + H^+ \longrightarrow H_2O + Fe^{3+} + OH\cdot \tag{2.19}$$

Additionally, the $H\cdot$ and $HO_2\cdot$ can oxidize Fe^{2+} by the following reactions [33]:

$$H\cdot + Fe^{2+} + H^+ \longrightarrow Fe^{3+} + H_2 \tag{2.20}$$

$$HO_2\cdot + Fe^{2+} + H^+ \longrightarrow H_2O + Fe^{3+} + H_2O_2 \tag{2.21}$$

The concentration of ferric ions (Fe^{3+}) can then be measured at a maximum absorption wavelength of 304 nm spectrophotometrically. Here, the molar absorptivity is estimated to $\epsilon = 2197\ M^{-1}cm^{-1}$ [16], [28].

2.6.3 Terephthalic Acid Dosimetry

Terephthalic acid (TA) dosimetry is considered an accurate method of determining the $OH\cdot$ concentration. This is because its product is exclusively produced by the hydroxyl radicals [34]. 0.332 g (0.002 mol) of TA and 0.200 g (0.005 mol) of NaOH is dissolved in water to make a solution with a pH of 7.4. A phosphate buffer made by 0.589 g (0.0044 mol) of KH_2PO_4 and 0.981 g (0.007 mol) of Na_2HPO_4 is then added to maintain the pH level. Deionized water is then added until a final solution volume of 1 L. During sonication the $OH\cdot$ combines with the dissolved terephthalate anions to form 2-hydroxyterephthalate (HTA) anions. The main reaction forming HTA is shown in Figure 2.4. However, this reaction process is more complex and is elucidated by Mark et al. [35].

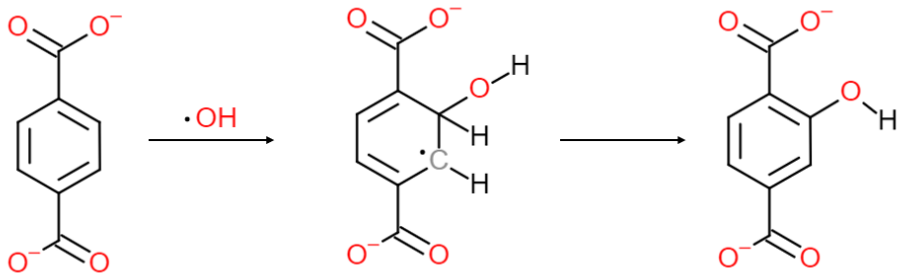

Figure 2.4: Scheme of the main reaction between TA anions and $OH\cdot$ to form HTA anions.

The HTA ions are highly fluorescent, making it possible to determine its concentration with fluorescence spectroscopy at an excitation wavelength of 315 nm, and an emission wavelength of 425 nm [16], [36].

2.6.4 Salicylic Acid Dosimetry

Salicylic acid is an organic compound just like terephthalic acid. This dosimeter is also accurate since its product is exclusively formed by hydroxyl radicals. In Figure 2.5 the reaction between the $OH\cdot$ and salicylic acid during sonication is illustrated. The main reaction is considered to be the hydroxylation of the 3^{rd} and 5^{th} bond in the aromatic ring, forming 2,3-dihydroxybenzoic acid (2,3-DHB) and 2,5-dihydroxybenzoic acid (2,5-DHB). Which of the two is dominant is reported to be dependent on whether the oxidation process is chemical or biological. In some cases, catechol is also considered as a main product [34].

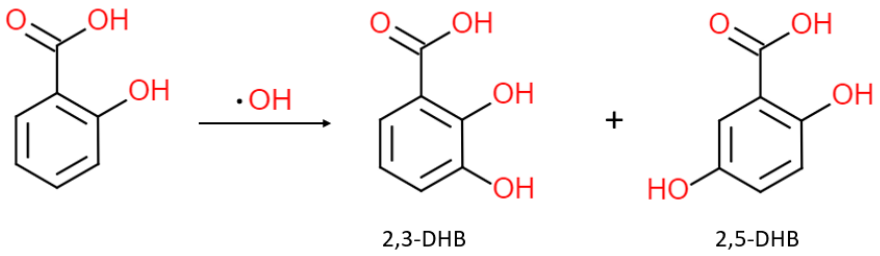

Figure 2.5: Scheme of reaction between salicylic acid and hydroxyl radicals to form 2,3-DHB and 2,5-DHB

A 1 L salicylic stock solution of 500µM can be made by mixing 0.6906 g (0.005 mol) of salicylic acid with deionized water until 1 L is obtained. To remove impurities, samples should be filtered through a 0.2 µm PFTE-filter [34]. The HPLC could be equipped with either a UV-Vis or a fluorescence detector.

For the fluorescence detector, a mobile phase of an 85:15 mixture consisting of an aqueous solution and methanol could be used. The aqueous solution consists of a 0.2% acetic/acetate buffer, which maintains a pH value of 5.9. Here, the flow rate used for the mobile phase is 0.7 mL/min, and a column length of 100 mm. The wavelengths chosen for the fluorescence measurements was $\lambda_{emission} = 448$ nm and $\lambda_{excitation} = 324$ nm. These should be determined by obtaining fluorescence spectra for salicylic acid, 2,3-DHB, and 2,5-DHB. Thus, both of the latter two products should be provided prior to experiments [34].

As for the UV-Vis detector, the mobile phase could consist of a 60:40 mixture of aqueous phosphoric acid solution (0.2M, pH 2.5) and methanol. The flow rate used for the mobile phase is given to be 1.0 mL/min. The maximum absorbance wavelength is $\lambda_{max} = 325$ nm. Calibration curves should be established with standard solutions of salicylic acid, 2,3-DHB and 2,5-DHB [37].

2.6.5 Methyl Orange Dosimetry

The methyl orange (MO) dosimetry method is based on the removal of the dissolved hydrophilic methyl orange ($C_{14}H_{14}N_3NaO_3S$) in water during sonication and has been used to study the degradation of organic pollutants [38]. Therefore, the method is not often applied when determining radical yield. MO has been shown to react with $OH\cdot$ by the reactions 2.22 and 2.23 [39]. The main reaction pathway for an azo dye like MO is the addition of $OH\cdot$ to the double bonds of the azo group [40]. Here, Z constitutes all species that react with $OH\cdot$ (Y etc.), except MO. V is the product from this reaction.

$$MO + OH\cdot \longrightarrow Y \tag{2.22}$$

$$OH\cdot + Z \longrightarrow V \tag{2.23}$$

The MO concentration left after sonication can be determined using a UV spectrophotometer at $\lambda_{max} = 463$ nm [40]. By subtracting the resulting MO concentration from

the initial concentration, MO degradation is obtained. In this way, one can quantify the H_2O_2 or $OH\cdot$ produced during sonication.

2.6.6 Nitric Acid Dosimetry

Nitric acid dosimetry is based on the formation of nitrous acid (HNO_2) during sonication of a nitric acid (HNO_3) solution. By following the HNO_2 formation, one can determine the H_2O_2 or $OH\cdot$ generated during sonication. For this quantification to be possible, the nitric acid solution needs to be accommodated by an anti-nitrous reactant such as hydrazinium nitrate $N_2H_5NO_3$ or sulfamic acid HN_2SO_3H. These species scavenge the HNO_2 by reaction 2.24 and 2.25, before the HNO_2 reacts with the H_2O_2 as reaction 2.26 shows. Furthermore, the formation of H_2O_2 is described in reaction 2.27 and 2.28, where one hydroxyl radical is involved in each hydrogen peroxide formation. Other species like NO_x is also formed during sonication [15].

$$N_2H_5{}^+ + 2\,HNO_2 \longrightarrow N_2O + N_2 + 3\,H_2O + H^+ \tag{2.24}$$

$$HNO_2 + HN_2SO_3H \longrightarrow N_2 + H_2O + H_2SO_4 \tag{2.25}$$

$$HNO_2 + H_2O_2 \longrightarrow HNO_3 + H_2O \tag{2.26}$$

$$NO_3{}^- + H^+ + OH\cdot \longrightarrow NO_3\cdot + H_2O \tag{2.27}$$

$$NO_3\cdot + H_2O \longrightarrow NO_2 + H_2O_2 \tag{2.28}$$

After sonication, each sample (0.1-1 mL) is filtered and mixed with aqueous solutions of: *(1)* 1 mL of 2.00 M NaOH, *(2)* 1 mL of a 100 mL solution made of 0.0345 M sulfanilic acid and 20 mL HNO_3, *(3)* 3 mL of a 100 mL solution made of 0.0419 M α-naphtylamine and 5 mL HCl, and *(4)* 5 mL of a 500 mL solution made of 0.8 M CH_3COONa and 3.2 M of $CH_2Cl-COOH$. This procedure is known as the Griess method. The colorimetric complex formed in the resulting 10 mL solution is subsequently analysed, and the HNO_2 can be quantified by UV-Vis spectroscopy at $\lambda_{max} = 535$ nm, and $\epsilon = 41\ 500\ \text{cm}^{-1}\text{M}^{-1}$ [15].

2.6.7 Titanyl Sulfate Dosimetry

For the titanyl sulfate dosimeter, pure water is sonicated. Samples, containing H_2O_2, is extracted and filtered with a 0.2 µm PTFE-filter. The samples is then mixed (1:1) with a solution made up by $1.2 \cdot 10^{-3}$ M (0.330 g) $TiOSO_4$ stirred in 100 mL of purified water. This solution should be gently heated in 3.5 mL of H_2SO_4 before the samples are added. A peroxotitanium (IV) complex, which is a colorimetric compound exhibiting an orange-yellow color, is formed during the mixing of the sample and the premade solution. The mixture is then analysed with a UV-Vis spectrometer at $\lambda_{max} = 410$ nm and a molar extinction coefficient of $\epsilon = 698\ \text{M}^{-1}\text{cm}^{-1}$ [15].

2.6.8 Coumarin Dosimetry

The coumarin dosimeter is based on sonication of coumarin ($C_9H_6O_2$) solution. In order to make a typical 1 L solution, simply mix 0.14614 g (1 mM) of pure coumarin in deionized water until 1 L is obtained. Upon sonication, the coumarin reacts with the hydroxyl radicals to form umbelliferone. A scheme of this reaction is seen in Figure 2.6.

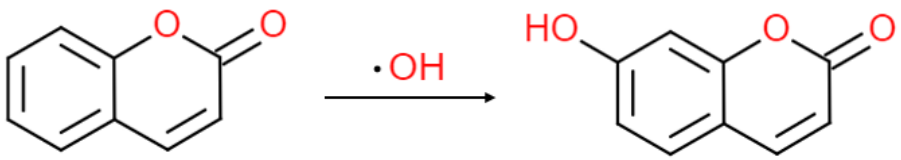

Figure 2.6: Scheme of reaction between coumarin and hydroxyl radicals to form umbelliferone

The umbelliferone can be detected by fluorescence spectroscopy at an excitation wavelength of 332 nm and an emission wavelength of 455 nm. It is reported that for different pH values, the emission wavelength shifted from 480 nm (pH = 1) to 455 nm (pH = 6). This occurs due to the chemical equilibrium between umbelliferone and protonated umbelliferone (see Figure 2.7). In addition, the reduction in coumarin could be measured using a UV-Vis spectrometer at $\lambda_{max} = 275$ nm and a molar extinction coefficient calculated from known concentrations of coumarin [41].

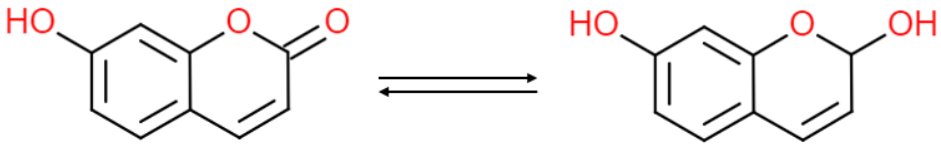

Figure 2.7: Scheme of chemical equilibrium between umbelliferone and protonated umbelliferone in acidic conditions

2.7 Characterisation Tools for Dosimetry Methods

Depending on the chemical produced by the reaction between the reactive species and its scavenger, one can measure its concentration in a solution by using methods like UV-Vis spectroscopy, fluorescence spectroscopy, or High Performance Liquid Chromatography (HPLC). Which of these methods to choose is dependent on the chemical properties of the product. Only the tools relevant to the dosimetry methods mentioned in Section 2.6 are included below. Many other characterisation tools for identification and quantification of compounds, such as mass spectroscopy, also exist.

2.7.1 UV-Vis Spectroscopy

UV-Vis spectroscopy is the study of the electromagnetic absorption of chemical species in the ultraviolet-visible spectrum [42]. The typical functioning of a UV-Vis spectrophotometer is relatively straightforward and illustrated in Figure 2.8.

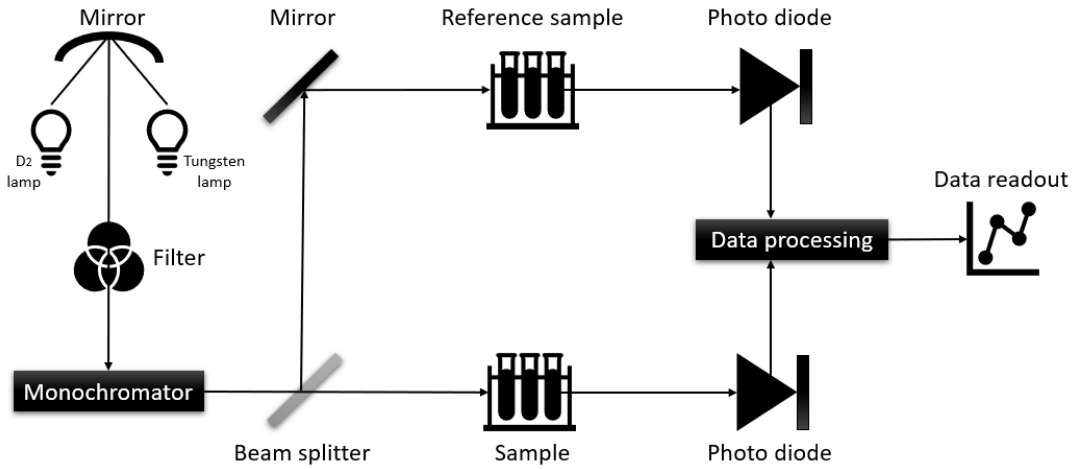

Figure 2.8: Typical functioning of a UV-Vis spectrophotometer

A UV or visible light source is split into particular wavelengths by using a diffraction grating or prism. By using a half mirror device, the monochromatic beam is further split into two beams with equal intensities. One beam travels through a small transparent reference cuvette containing only the solvent, while the other travels through a cuvette containing the sample solution. Electronic detectors measure the adjoining light intensities I_0 and I [43], [44]. The transmittance (T) of the light through the cuvette can then be determined by:

$$T = \frac{I}{I_0}. \tag{2.29}$$

The absorption of light in the sample is defined as the logarithm of the reciprocal of the transmittance:

$$A = log\ \frac{1}{T} = -log\ \frac{I}{I_0}. \tag{2.30}$$

Usually, the absorption at a specific wavelength is measured from 0 to 2, corresponding to 100% and 1% transmittance, respectively. If the measured absorption is very high, dilution of the sample may be needed to obtain correct results. For analysis below 280 and 320 nm, plastic and glass cuvettes are no longer viable, respectively. Preferably, quartz cuvettes should be used instead [45].

Different compounds may have different absorption characteristics and maxima. By determining the maximum absorption wavelength, λ_{max}, one can determine the unknown concentration of a specific compound using the Beer-Lambert law:

$$A = \epsilon \cdot l \cdot c, \tag{2.31}$$

where A is absorption, ϵ is the molar extinction coefficient (or *molar absorptivity*) in $dm^3mol^{-1}cm^{-1}$, l is the distance the light travels through the solution in cm, and c is the concentration of the absorbing species in mol/L. The molar extinction coefficient

can either be found in literature or determined by measuring the absorption of known concentrations [46].

2.7.2 Fluorescence Spectroscopy

Fluorescence spectroscopy is a type of electromagnetic spectroscopy that analyses the fluorescence in a sample. Many parameters can be analysed, and the most common include excitation spectra, emission spectra, fluorescence lifetimes, quantum yield, and anisotropy [47]. In relation to the field of sonochemistry and dosimetry, the first two is the most relevant. Devices that measure the level of fluorescence are called spectrofluorometers, and their typical functioning is illustrated in Figure 2.9.

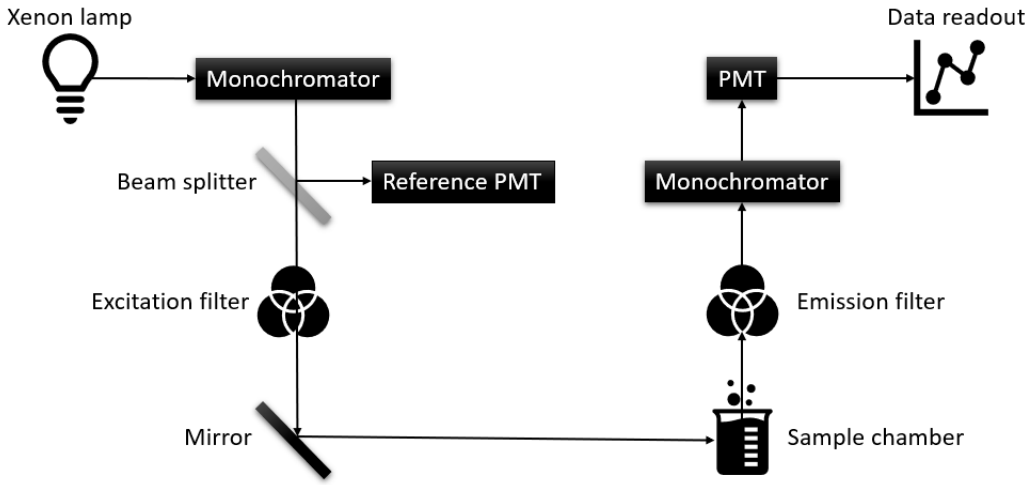

Figure 2.9: Typical functioning of a fluorescence spectrophotometer

A high-pressure xenon arc lamp is usually used as a light source. The lamp emits a continuous spectrum of light, usually in the range 250-1100 nm. The light is sent through what is called the excitation monochromator which passes the light at a specific wavelength, meant for irradiating the sample. This wavelength is often described as the excitation wavelength ($\lambda_{excitation}$). When the light passes through the sample, some light is absorbed. This causes the molecules or atoms in the sample to move from its ground state to an excited state. After a fluorescence lifetime, the molecules or atoms have decayed from their excited states to the ground state. In this process, light (or *fluorescence*) is emitted. These processes are further explained by what is known as the Perrin Jablońsky diagram. The emitted light from the samples passes the emission monochromator, which filters out light except that of wavelength $\lambda_{emission}$. Here, the wavelength with maximum fluorescence is chosen. When the light reaches the detector, the fluorescence signal is converted into a current by a photomultiplier tube (PMT), and to a screen for data readout [47], [48].

2.7.3 High Performance Liquid Chromatography

High Performance Liquid Chromatography (HPLC) is a method for separating, identifying, and quantifying compounds in a mixture. HPLC differs from liquid chromatography due to its high operational pressure, and employment of stationary phases. The technique

is considered to be highly accurate. In Figure 2.10, the basic workings of an HPLC is presented.

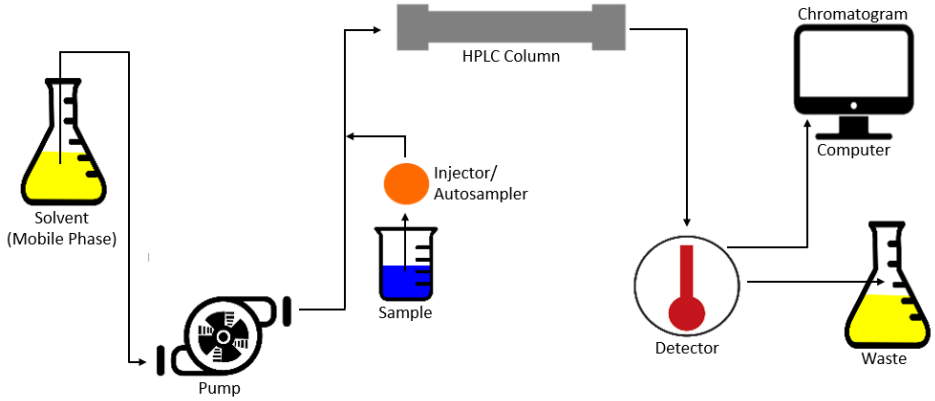

Figure 2.10: Typical functioning of a HPLC

A mobile phase, made up from a solvent, is driven through a pump which applies sufficient force on the solvent so that it passes through the stationary phase. The sample to be analysed is injected into the mobile phase by a manual injector or autosampler. It is vital that the sample to be analysed is able to dissolve in the mobile phase. The stationary phase or column is made up by tiny particles (a solid or a liquid on a solid support). During the interaction between the mobile phase and the stationary phase, the sample compounds get separated from each other. The physical effect causing the separation process varies. For a liquid-solid system, the separation is due to dipole-dipole interactions between the sample compounds and the particles in the stationary phase. Following separation, the mobile phase reaches the detector, which quantifies the separated compounds. The detector can, for instance, be a UV-Vis spectrophotometer, a spectrofluorometer, or a mass spectrometer. This device sends measurement signals to computer software that converts them into a chromatogram [49], [50], [51].

3 Problem Description

The main objective of this thesis is to study the effects of ultrasonic frequency, acoustic power, and liquid height on radical yield in a sonochemical reactor. Mainly, the experiments can be divided into three segments - First, the determination of acoustic power by calorimetry - Subsequently, the effect of liquid height and lastly, the effect of ultrasonic frequency and acoustic power.

As the determination of the acoustic power is essential to calculate SE (see Section 2.6), it was determined for all variations of amplitude, frequency, and liquid height used in this thesis through calorimetry. The SE is crucial as it makes it possible to compare results with similar conditions but varying acoustic powers. More than 120 calorimetric experiments were performed in this segment.

The effect of liquid height on radical yield is connected to the geometry of the reaction vessel (see Section 2.5.5), and only some research to study its effect have been undertaken [24]. Also, it is reported that only small changes in the reactor geometry can cause noticeable changes in sonochemical activity, making it particularly interesting to study [20], [21]. It is expected that the radical yield will increase as liquid height is increased. Because the reaction vessel provided for the work in this thesis was long and cylindrical shaped, it was excellent for testing liquid height while maintaining a constant cross-sectional area. The effect of liquid height was studied with five different heights under four frequencies of 24 kHz, 580 kHz, 860 kHz, and 1140 kHz. The amplitude remained constant at 100% during the experiments, and the liquid was cooled during operation by a water circulation system. For this segment, a total of 40 experiments were executed, all without gas saturation.

Ultrasonic frequency is reported to have a substantial impact on the radical yield, with an optimal frequency between 200-600 kHz [7]. However, most sonochemical studies have been done at 20 kHz [2]. Hence, experimenting with several frequencies under similar conditions may reveal some of its behavior and characteristics. The frequencies were chosen based on available equipment and were 24 kHz, 580 kHz, 860 kHz, and 1140 kHz. Additionally, the liquid was saturated with argon gas for 10 minutes before sonication, as it has been reported to improve the sonochemical yield due to its high polytropic ratio, low thermal conductivity, and high solubility [18]. Amplitudes of 20%, 40%, 60%, 80%, and 100% were used for all frequencies, in order to study the effect of acoustic power. An increase in sonochemical activity is expected as the amplitude is increased. A total of 120 experiments were performed for this segment, using the same water circulation system as mentioned earlier.

As for dosimetry methods, the Weissler and Fricke dosimeter were used. Although these methods are not as accurate as the terephthalic acid and salicylic acid dosimeter, they were chosen due to their reliability, simplicity, and cost. Besides, UV-Vis spectroscopy was the only available characterisation tool for this thesis.

4 Experimental Procedure

Two ultrasonicators were used in the experiments. These were the Meinhardt Ultrasonics Multifrequency System (580 kHz, 860 kHz, and 1140 kHz) and the Hielscher UP400St (24 kHz). The multifrequency system uses a plate transducer, while the Hielscher uses a sonotrode.

The multifrequency system is made up of a plate transducer that was attached underneath a cylinder glass vessel, also provided for Meinhardt Ultrasonics. This vessel is made up of an outer part for circulation cooling and an inner part for the reaction solution. The plate transducer provides direct sonication to the reaction solution. The cooling vessel has two connections at the top and bottom, used as inlet and outlet. A picture of the system can be seen in Figure 4.1.

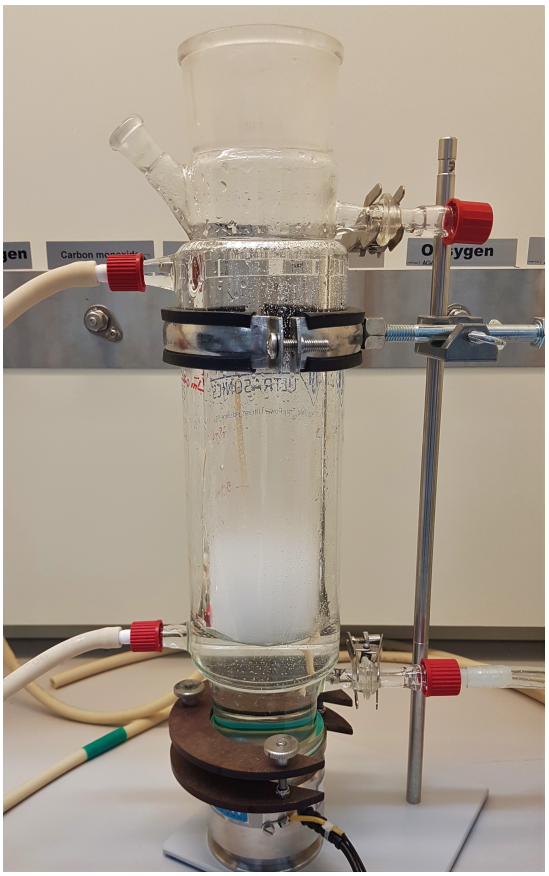

Figure 4.1: Meinhardt system and glass reaction vessel during sonication with argon saturation and cooling. The mist seen above the liquid occurs during sonication at higher frequencies.

The setup used for the Hielscher ultrasonicator was customised to have the same geometry as the multifrequency setup mentioned above. This was done in order to get comparable results. For experiments with less liquid height, a beaker with corresponding diameter submerged in cooling water was used. The Meinhardt Ultrasonics glass vessel was used for experiments where the liquid height was high enough to submerge the sonotrode into the glass vessel. Pictures of these two setups are seen in Figure 4.2.

For the dosimetry experiments, the Julabo MW-12 was used for temperature control. The system contained about 12 L of distilled water maintained at 25 °C, and circulated using

(a) **(b)**

Figure 4.2: (a) Hielscher ultrasonicator setup for higher liquid levels (625 mL and 750 mL), (b) Hielscher ultrasonicator setup for lower liquid levels (250 mL, 375 mL, and 500 mL)

a pressure and suction pump. It was used mainly to reduce the temperature increase in the reaction vessel during sonication. In such a way, temperatures in the reaction vessel only varied with a few degrees during the experiments. The circulation system was connected to the glass vessel by plastic tubes, tightened by tube clamps. In order to ensure no leakage, several test runs where performed.

4.1 Determination of Acoustic Power by Calorimetry

As mentioned in Section 2.5.1, the determination of acoustic power is essential when comparing sonochemical results. Each calorimetric experiment included one-minute sonication of deionized water. Temperature measurements were done by using two wire thermocouples connected to the National Instruments cDAQ-9172 socket. Software for recording the temperature each second was programmed in the system engineering software called LabView and is seen in Figure 4.3. During experiments, both thermocouples were placed in the middle of the liquid in order to obtain the mean temperature in the liquid. Each experiment was then performed three times (one-minute sonication) for the relevant liquid height, amplitude, and frequency. In order to determine the acoustic power, more than 120 calorimetric experiments were performed.

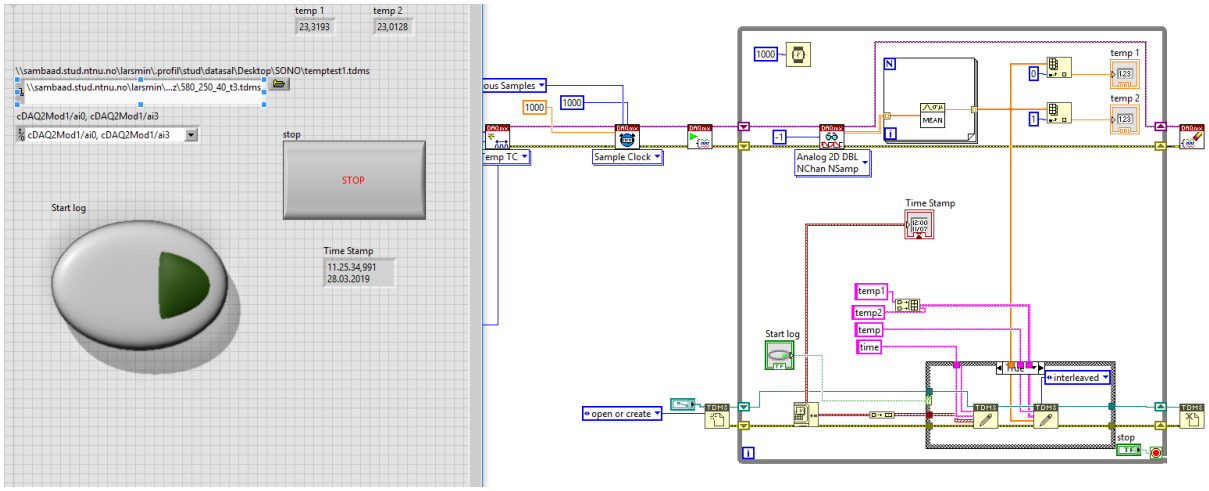

Figure 4.3: Program for temperature recording made in LabView. The software reads the input from the cDAQ-9172 socket, and saves it to an Excel file after logging is initiated.

4.2 Calibration of DO-meter and pH-meter

A DO-meter (Dissolved Oxygen) and a pH-meter provided from Hanna Industries, were used respectively during gas saturation and preparation of Fricke solution. For accurate measurements, these meters needed proper calibration less than one week before use.

The DO-probe was initially prepared by inserting an o-ring into the membrane cap, before rinsing and filling it with accompanying electrode solution. The membrane cap was tapped to dislodge any gas bubbles. It was then screwed onto the probe such that the platinum cathode faced down towards the PFTE-filter. Furthermore, the DO-meter got calibrated with two calibration points at 0% and 100% oxygen saturation. The zero oxygen calibration solution was prepared by mixing a dry chemical reagent and a solvent, and used for the first calibration point. For the second at 100% saturation, the probe was held directly above a beaker of water as described in the manual. When not in use, the DO-probe was stored in a protective cap.

The pH-meter was calibrated with three buffer solutions with pH 7.01, 4.01, and 10.01 delivered from Hanna Industries. Three buffers were recommended for accurate measurements. Small amounts of each buffer solution were poured into three plastic beakers. The pH-meter was calibrated by submerging the probe about 3 cm into the buffer solutions. An additional three beakers with cleaning solution were used for cleaning the pH-probe between each calibration point. A storage solution for pH electrodes along with a protective cap were used when the probe was not in use.

4.3 Preparation and Disposal of Fricke and Weissler Solutions

All chemicals were provided by Sigma-Aldrich. For half of the experiments, a Weissler solution of 0.1 M was prepared by dissolving 16.600 g/L of KI, with a molecular weight of 166.00 g/mol, in deionized water. The ACS reagent graded potassium iodide of purity $\geq$ 99 % was weighed using the VWR SE203-LW, which uses precision balances and draught shield.

For the Fricke solution, the ACS Reagent graded sulfuric acid of 95-98 % w/w needed to be diluted before use. Due to its strong acidity, the dilution was performed inside

a fume hood with great caution, to avoid any accidents. With a density of 1.84 g/mL, and a formula weight of 98.08 g/mol, a 4 M solution was made by slowly adding 441.9 mL of stock solution to 1 L of deionized water. During this process, a cooling bath and a magnetic stirrer was used to avoid extensive heating of the solution, which occurs due to exothermic reactions between the sulfuric acid and water. The final volume of the solution was then adjusted with deionized water until 2 L was obtained. In order to guarantee a correct concentration, the pH was measured using the Hanna Industries pH-meter and corresponded to the calculated pH value of a strong acid:

$$pH = -log_{10}([\mathrm{H}^+]) = -log_{10}([\mathrm{H_2SO_4}]) = -log_{10}(4) = -0.60. \tag{4.1}$$

After dilution, 0.117 g of sodium chloride and 0.784 g of ammonium iron(II) sulfate hexahydrate was weighed and mixed with 1 L distilled water inside a volumetric flask. 255.5 g of the 4 M sulfuric acid solution was then added before the volume was adjusted to 2 L by deionized water. In this way, the mixing of the Fricke solution corresponded to the recipe mentioned in Section 2.6.2.

All solutions used for the Weissler and Fricke experiments, including the unsonicated samples were allocated to a plastic container at the laboratory for disposal and marked according to the solution type and concentration. In such a way, the chemicals were handled according to the safety data sheets and laboratory rules. Reusable equipment in contact with solution was regularly cleaned, especially when in contact with the very acidic Fricke solution. Disposable plastic beakers, cuvette, and pipettes, was emptied thoroughly before disposal.

4.4 Determination of Optimal Liquid Height

As mentioned in Section 2.5.5, one of the parameters affecting the sonochemical yield is the liquid level of the reaction vessel. To determine the optimal liquid height in terms of sonochemical efficiency, different amounts of solution was used. In such a way, sonochemical efficiencies could be calculated for various frequencies and liquid heights. In Table 4.1, the various experiments performed is listed. Totally, 40 experiments were executed, and 80 samples were taken. All experiments where performed with cooling and five minutes of sonication.

Table 4.1: Experiments performed to determine optimal liquid heights

Frequency [kHz]	Volume [mL]	Liquid height [mm]
24	250	85.7
24	375	121.5
24	500	148.6
24	625	185.1
24	750	222.0
580	250	85.7
580	375	121.5
580	500	148.6
580	625	185.1
580	750	222.0
860	250	85.7
860	375	121.5
860	500	148.6
860	625	185.1
860	750	222.0
1140	250	85.7
1140	375	121.5
1140	500	148.6
1140	625	185.1
1140	750	222.0

The experiments shown in Table 4.1 was performed both for the Weissler and Fricke dosimeter. In order to determine the liquid height corresponding to a specific volume, a digital capiler was used. As mentioned earlier in this section, a beaker with diameter equal to the Meinhardt Ultrasonics cylinder glass vessel was used for the 24 kHz experiments at lower liquid heights, more specifically 85.7, 121.5, and 148.6 mm.

4.5 Determining the Effect of Frequency and Acoustic Power

In order to determine the effect caused by frequency and acoustic power for this sonochemical setup, four different frequencies of 24, 580, 860, and 1140 kHz were studied at amplitudes of 20, 40, 60, 80, and 100%, in almost identical environments. Due to the results obtained by studying the effects of liquid height, 250 mL (liquid height of 85.7 mm) of both the Weissler and Fricke solution was used for these experiments. Each experiment was repeated three times, with a sonication time of five minutes. In addition, the cooling system mentioned in Section 4 was used to avoid significant temperature changes. Totally, 60 experiments for each dosimetry method where performed, resulting in 120 experiments and 240 samples (before and after sonication). The various setups and parameters for the experiments are shown in Table 4.2.

Due to the beneficial effects caused by a high polytropic ratio and low thermal conductivity of argon gas, all experiments involved argon saturation for ten minutes before sonication. The gas was bubbled through the solution using a gas pipe connected to the lower part of the glass reaction vessel. Some initial tests using the DO-meter were done to confirm that the solution contained no oxygen and was saturated with argon. The

gas was provided by the Department of Energy and Process Engineering at NTNU, and available through gas pipes connected directly to the fume hood.

Table 4.2: Experiments performed to determine effect of frequency and acoustic power. All experiments were performed three times for both Weissler and Fricke dosimetry, with 250 mL solution, argon saturation, cooling, and a sonication time of five minutes.

Frequency [kHz]	Amplitude [%]	Transducer	Reaction Vessel
24	100	Hielscher	Borosilicate beaker
24	80	Hielscher	Borosilicate beaker
24	60	Hielscher	Borosilicate beaker
24	40	Hielscher	Borosilicate beaker
24	20	Hielscher	Borosilicate beaker
580	100	Meinhardt	Meinhardt glass vessel
580	80	Meinhardt	Meinhardt glass vessel
580	60	Meinhardt	Meinhardt glass vessel
580	40	Meinhardt	Meinhardt glass vessel
580	20	Meinhardt	Meinhardt glass vessel
860	100	Meinhardt	Meinhardt glass vessel
860	80	Meinhardt	Meinhardt glass vessel
860	60	Meinhardt	Meinhardt glass vessel
860	40	Meinhardt	Meinhardt glass vessel
860	20	Meinhardt	Meinhardt glass vessel
1140	100	Meinhardt	Meinhardt glass vessel
1140	80	Meinhardt	Meinhardt glass vessel
1140	60	Meinhardt	Meinhardt glass vessel
1140	40	Meinhardt	Meinhardt glass vessel
1140	20	Meinhardt	Meinhardt glass vessel

4.6 Sample Analysis by UV-Vis Spectroscopy

Samples were taken before and after sonication by using either reusable plastic syringes or disposable pipettes. The samples taken before sonication were used as reference or zero base for the ones taken after sonication. Each sample was kept in a small airtight plastic container to avoid contamination and named according to its respective experiment for easy identification. The plastic syringes were cleaned several times with deionized water and air-dried before reuse. Plastic cuvettes with a standardized light path length of l = 1 cm were used in the analysis of both Weissler and Fricke experiments. To ensure correct measurements, the cuvettes were handled with nitrile gloves to avoid fingermarks and checked for air bubbles before analysis.

As previously described in Section 2.6.1, the quantity of I_3^- ions can be determined by UV-Vis spectroscopy at a maximum absorption wavelength of 350-355 nm. For the Weissler experiments, a maximum was seen at 350 nm and thus analysed at this wavelength, using the Thermo Scientific Genesys 30 Visible Spectrophotometer. As for the Fricke dosimetry, a maximum absorption wavelength for Fe^{3+} was seen at 304 nm, corresponding to that found in the literature (see Section 2.6.2). As the Thermo Scientific Genesys 30 had a lower analysing limit of 325 nm, the Spectronic Helios Gamma UV-Vis Spectrophotometer by Thermo Fisher Scientific was used for the Fricke samples.

5 Results and Discussion

In the following subsections, the results of this thesis are presented and discussed. In Section 5.1 the results for calorimetry is presented. Further, the results for the determination of optimal liquid height is found in Section 5.2. Lastly, the effect of frequency and acoustic power on sonochemical activity is presented in Section 5.3, with additional data on the argon saturation process.

The results which includes the use of Weissler and Fricke dosimetry is presented in terms of the I_3^- and Fe^{3+} concentration, which is coherent with several papers [16], [24], [28]. As described in Section 2.6.1 and 2.6.2, both the I^- and Fe^{2+} can be oxidized by both $OH\cdot$ and H_2O_2, along with other reactive species. Fang et al. [33] emphasized this aspect for the Fricke dosimeter. Thus, it was chosen not to present the results in terms of $OH\cdot$ and H_2O_2 concentration, although there is examples of papers [8] that presents their results in this manner.

5.1 Determination of Acoustic Power by Calorimetry

For each calorimetric experiment, the measured temperature change from the two thermocouples during sonication were averaged in Excel and plotted over a period of one minute. By averaging, a more representative result can be obtained, due to local variations in temperatures and measurement disturbances that may occur during sonication. To obtain $dT/dt|_{t=0}$, curve fitting (second order polynomial) was used to obtain the curve fitting line equation. A plotted example of such curve fitting can be found in Appendix A, Figure A.1. This equation was then differentiated and evaluated at t=0. Furthermore, the three values obtained for $dT/dt|_{t=0}$ for each calorimetric setup were averaged. Lastly, the acoustic power was calculated using equation 2.8. Here, $c_p = 4182$ J/kg·K, and $\rho = 0.998$ kg/m^3 [52]. Both of these liquid properties are assumed constant. This assumption is valid due to the accuracy of the experiments and the relatively small temperature change observed. A summary of the calculated acoustic power (P) is to be found in Table 5.1.

Table 5.1: Calculated acoustic power for various sonochemical setups (V = volume, A = amplitude, P = acoustic power at given frequency)

V [mL]	A [%]	P_{24kHz} [W]	P_{580kHz} [W]	P_{860kHz} [W]	$P_{1140kHz}$ [W]
250	100	149.24	47.65	51.54	52.38
250	80	116.48	30.22	27.02	31.16
250	60	88.76	16.56	16.10	15.79
250	40	56.41	3.76	2.92	2.71
250	20	19.30	~ 0	~ 0	~ 0
375	100	146.7	51.13	52.64	56.92
500	100	155.33	55.09	55.72	58.99
625	100	149.90	56.00	52.00	54.08
750	100	160.58	58.54	54.99	63.96

It is important to notice that the acoustic power for 24 kHz is much higher than those of higher frequency. This is due to transducer differences (Hielscher and Meinhardt). Ultrasonic horn-type transducers producing lower frequencies and that utilizes a sonotrode,

are usually able to operate at higher powers than those made for higher frequencies (plate transducers). This occurs due to the amplification of intensity at resonance frequency when a BLT is connected with multiple metal pieces (see Section 2.3). Furthermore, it is worth mentioning that the initial water temperature during calorimetric experiments is irrelevant, being that constant properties is assumed, and due to how acoustic power is calculated. However, after the deionized water was poured into the reactor the liquid was given time to reach steady-state temperature before the experiments were initiated.

As seen in Table 5.1, the acoustic power at 20% amplitude for the Meinhardt multifrequency system is about 0 W for this type of sonochemical setup. This can indicate that no ultrasonic power is dissipated in the liquid, that the thermocouples used are unable to detect small temperature changes, or that the heat loss from the liquid to the surroundings is approximately equal to the dissipated ultrasonic energy. Moreover, the acoustic power was approximately linear for the Hielscher transducer, while the Meinhardt multifrequency system gave a more exponential increase in acoustic power with increasing amplitude. This can be seen below in Figure 5.1 and 5.2. It should be specified that the characteristics of Figure 5.2 also apply for the frequencies 860 kHz and 1140 kHz. As the sonochemical setup remained almost identical during the calorimetric experiments, the difference in characteristics between the Hielscher and Meinhardt transducers is most likely explained by their inner workings.

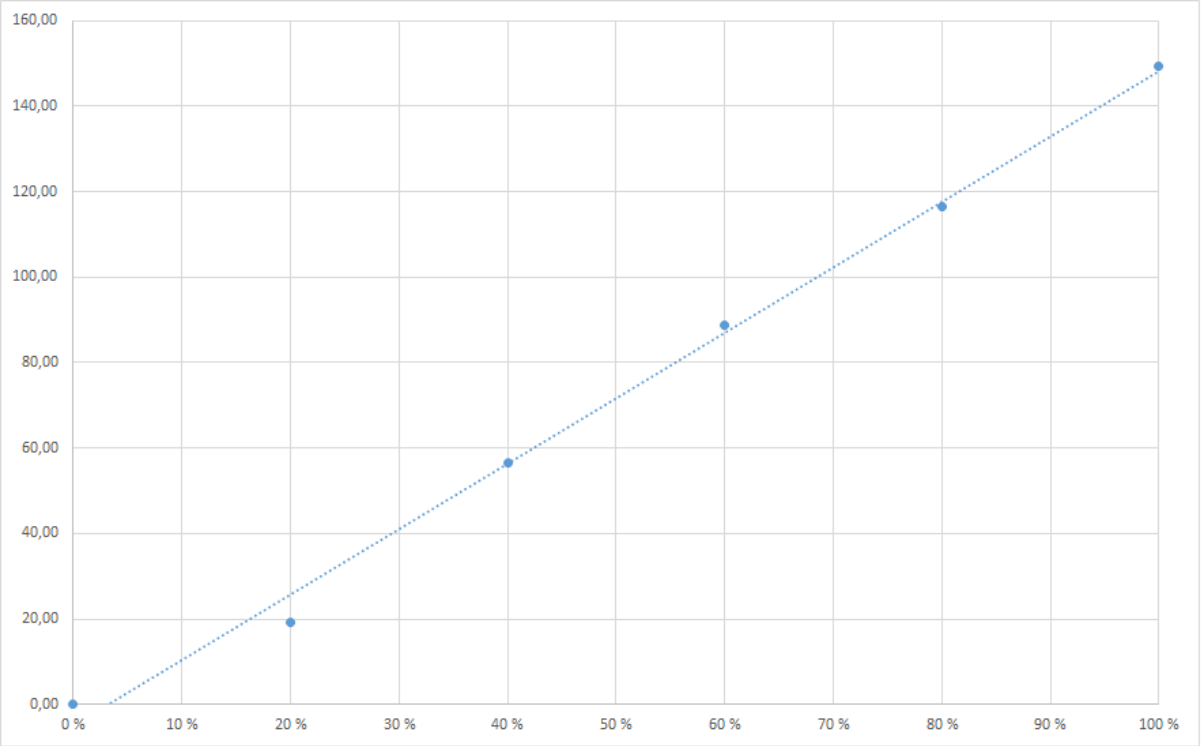

Figure 5.1: Plot of acoustic power vs. amplitude for the Hielscher transducer (24 kHz) at 250 mL and 100% amplitude. The dotted line is a linear curve fitting line.

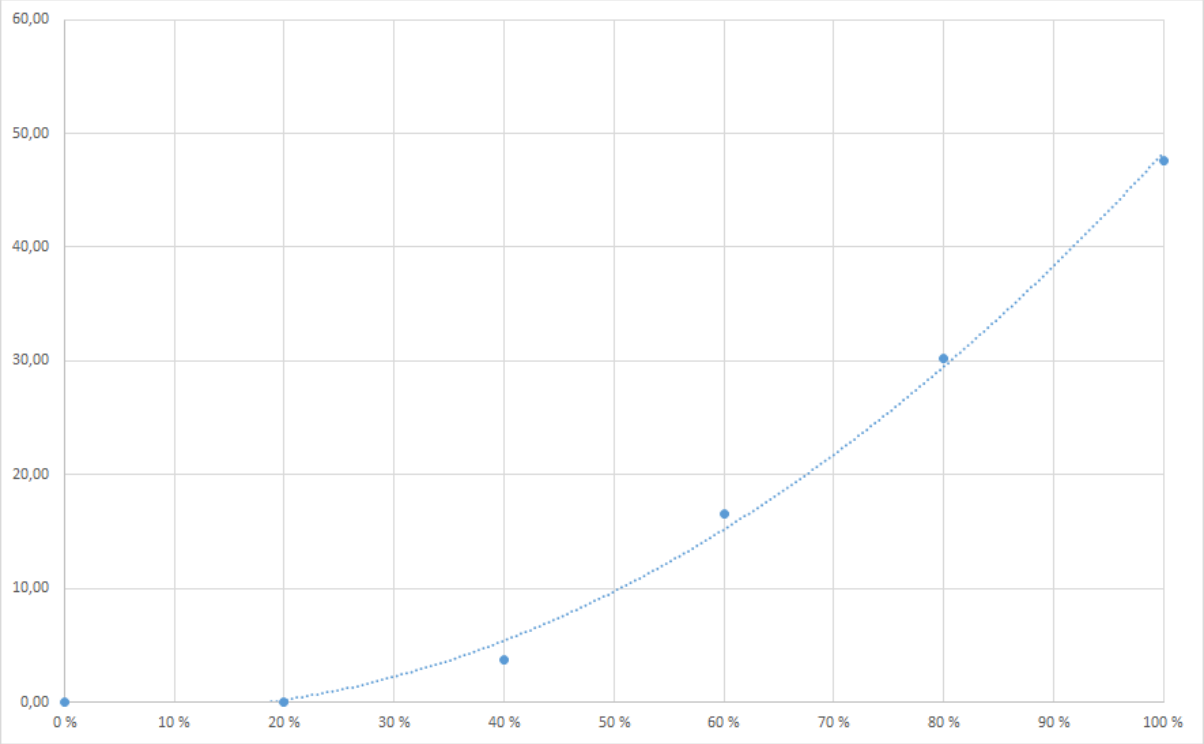

Figure 5.2: Plot of acoustic power vs. amplitude for the Meinhardt transducer (580 kHz) at 250 mL and 100% amplitude. The dotted line is a 2nd order polynomial curve fitting line.

Although it was expected that the acoustic power would increase with an increase in liquid height (due to more dissipation of ultrasonic energy), this was not the case for 625 mL at 860 and 1140 kHz. As acoustic cavitation is a complex phenomenon, it can be hard to identify the reason behind why this happens, and many elements need to be considered. For instance, the ultrasonic waves reaching the liquid-air interface are being completely reflected into the liquid. The ultrasonic waves are also reflected at the wall, but the reflection depends upon both wall geometry and material. The reflected waves create both constructive and destructive interference and affect acoustic intensity [6].

Additionally, there are ample amounts of attenuation of ultrasound in a bubbly solution due to a decrease in bulk density and sound velocity. Such changes cause the acoustic pressure amplitude of the wave to drop, which in turn cause the acoustic intensity to decrease. Thus, a drop in acoustic intensity below the threshold intensity (see Section 2.1) reduces the cavitation in the liquid. At higher frequencies the cavitation intensity threshold increases, and may be a meagre explanation of the reduction in acoustic power for 625 mL at 860 and 1140 kHz [6].

5.2 Determination of Optimal Liquid Height

In this thesis, the effect of liquid height was determined by SE (see Section 2.6), which is similar to the work done by Son et al. [21]. In such a way, the optimal liquid height is determined based on the highest production of I_3^- or Fe^{3+} per dissipated energy unit (acoustic power).

5.2.1 Weissler Dosimetry

The maximum absorption wavelength was observed at 350 nm for all the Weissler dosimetry experiments, and a typical absorption scan from 325-500 nm with this peak can be seen in Appendix A, Figure A.2. By using equation 2.31, with a molar absorptivity of ϵ = 26 000 $M^{-1}cm^{-1}$, and l = 1 cm, the concentration of I_3^- ions was calculated. Although this value is based on literature, it would be preferable to calculate it by using known concentrations of triiodide. However, this was not possible due to the chemicals available.

Finally, the SE was calculated based on equation 2.10 as well as the acoustic power presented in Table 5.1. The results obtained for the Weissler dosimetry method are shown in Table 5.2, and the optimal outcome for each frequency are marked with bold font.

Table 5.2: Results for studying the effect of liquid height using the Weissler dosimeter

f [kHz]	H [mm]	V [mL]	A_{350nm} [-]	[I_3^-] [µmol/L]	SE [µmol/kJ]
24	85.7	250	0.235	9.038	0.050
24	121.5	375	0.191	7.346	0.063
24	148.6	500	0.175	6.731	0.072
24	**185.1**	**625**	**0.140**	**5.385**	**0.075**
24	222.0	750	0.096	3.692	0.057
580	**85.7**	**250**	**0.968**	**37.231**	**0.665**
580	121.5	375	0.487	18.731	0.458
580	148.6	500	0.346	13.308	0.403
580	185.1	625	0.349	13.423	0.499
580	222.0	750	0.249	9.577	0.409
860	**85.7**	**250**	**0.740**	**28.462**	**0.460**
860	121.5	375	0.451	17.346	0.412
860	148.6	500	0.267	10.269	0.307
860	185.1	625	0.196	7.538	0.302
860	222.0	750	0.125	4.808	0.219
1140	**85.7**	**250**	**0.576**	**22.154**	**0.352**
1140	121.5	375	0.406	15.615	0.343
1140	148.6	500	0.289	11.115	0.314
1140	185.1	625	0.223	8.577	0.330
1140	222.0	700	0.131	5.038	0.197

As seen in Table 5.2, the optimal liquid height is seen at 625 mL (185.1 mm) for 24 kHz, and 250 mL (85.7 mm) for 580 kHz, 860 kHz, and 1140 kHz. Two observations are especially interesting. First, among the different frequencies, the highest SE is seen at 580 kHz for all liquid heights, which is consistent with the reported maximum radical yield between 200 and 600 kHz reported by Ashokkumar [7]. Second, the optimal liquid height is consistent among the higher frequencies using the Meinhardt plate transducer, while the optimal liquid height is much higher for the 24 kHz (with sonotrode). This may be explained by the differences in ultrasonic wave propagation between high and low frequencies. A higher amount of cavitation bubbles is found at the pressure antinodes of the ultrasonic wave, which is dependent upon the wavelength or frequency of the ultrasound [53]. In addition, the effects described in Section 5.1 concerning attenuation,

reflection, interference, and threshold intensity may explain why the SE is at its highest at 85.7 mm for higher frequencies.

5.2.2 Fricke Dosimetry

For the Fricke dosimetry, a maximum absorption wavelength was found at 304 nm, corresponding to that found in literature [16], [28]. Due to the features provided by the Spectronic Helios Gamma UV-Vis Spectrophotometer, it was not possible to extract a typical scan for the Fricke dosimeter similar to Figure A.2. By using equation 2.31, with a molar absorptivity of $\epsilon = 2\ 197\ \mathrm{M^{-1}cm^{-1}}$, and $l = 1$ cm, the concentration of Fe^{3+} ions was calculated. Although this molar absorptivity is found in literature, it would be preferable to calculate this value by using known concentrations of ferric ions. The SE was then calculated using the same procedure as mentioned in Section 5.2.1. Results concerning optimal liquid height using the Fricke dosimeter is presented in Table 5.3, with optimal liquid height results in bold font.

Table 5.3: Results for studying the effect of liquid height using the Fricke dosimeter

f [kHz]	H [mm]	V [mL]	A_{304nm} [-]	$[Fe^{3+}]$ [µmol/L]	SE [µmol/kJ]
24	**85.7**	**250**	**0.094**	**42.786**	**0.239**
24	121.5	375	0.051	23.213	0.198
24	148.6	500	0.048	21.848	0.234
24	185.1	625	0.037	16.841	0.234
24	222.0	750	0.028	12.745	0.198
580	**85.7**	**250**	**0.296**	**134.729**	**2.407**
580	121.5	375	0.169	76.923	1.881
580	148.6	500	0.093	42.330	1.281
580	185.1	625	0.085	38.689	1.439
580	222.0	750	0.063	28.675	1.225
860	**85.7**	**250**	**0.233**	**106.054**	**1.715**
860	121.5	375	0.108	49.158	1.167
860	148.6	500	0.059	26.855	0.803
860	185.1	625	0.035	15.931	0.638
860	222.0	750	0.027	12.289	0.559
1140	**85.7**	**250**	**0.171**	**77.833**	**1.238**
1140	121.5	375	0.097	44.151	0.970
1140	148.6	500	0.056	25.489	0.720
1140	185.1	625	0.038	17.296	0.666
1140	222.0	700	0.029	13.200	0.516

As seen in Table 5.3, all of the optimal heights are at 85.7 mm (250 mL). At 24 kHz these results differ from that observed in the Weissler experiments. Still, the SE results for the 24 kHz experiments for both the Weissler and Fricke dosimeter is quite similar. On such accounts, it would be preferable to repeat both the Weissler and Fricke dosimetry, and identify the uncertainty or standard derivation as done for the experiments in the following section. Nonetheless, it was not prioritized due to the time constraints in this thesis. Although the uncertainties are unknown, the results from the higher frequencies

of 580 kHz, 860 kHz, and 1140 kHz at 85,7 mm are clearly differing from the other results at those frequencies.

5.3 Determining the Effect of Frequency and Acoustic Power

The concentration and SE for the Weissler and Fricke dosimeter are calculated in the same manner as in Section 5.2. As mentioned in Section 4.5, each experiment was repeated three times. Consequently, it was possible to calculate the standard deviation (SD) based on the variation of the results. Equation 5.1 was used to calculate the SD.

$$\sigma = \sqrt{\frac{1}{N}\sum_{i=1}^{N}(x_i - \mu)}. \tag{5.1}$$

Here, σ is the SD, N = 3 (repeated experiments), x_i is the measured value for an experiment, and μ is the average of the three measured values. The SDs was relatively low for all Weissler dosimetry experiments, and highest at the Fricke dosimetry experiments, especially at 24 kHz. The SD will be discussed further in the following sections.

5.3.1 Argon Saturation

To ensure that both the Weissler and Fricke solution was argon saturated before sonication, the DO-meter was used to investigate if the argon replaced the oxygen dissolved in the solution, and how long this may take. From Figure 5.3, it can be seen that the concentration of oxygen in the solution is reduced to zero after about 410 seconds with argon bubbling. The initial increase in DO is most likely due to the air present in the gas pipe at the start of this process. Besides, the air close to the liquid-gas interface likely got mixed with the liquid, as the gas was bubbled through until the air above the liquid was replaced with argon gas. As a result of this investigation, the argon saturation process was set to ten minutes for all experiments.

In hindsight, a possible problem that may have affected the results is a possible degassing of argon during sonication. The argon saturation process was not continued during sonication. Hence, acoustic streaming and temperature increase which causes solubility to decrease, may cause degassing in the solution.

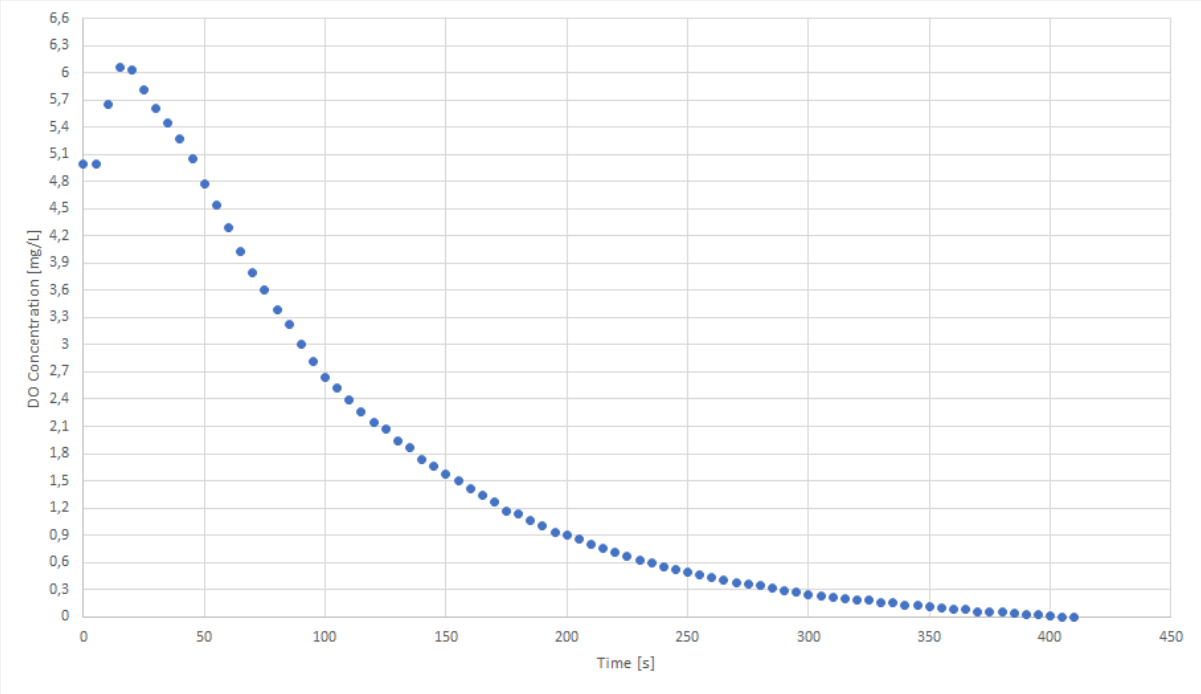

Figure 5.3: Reduction of dissolved oxygen in solution during argon saturation

5.3.2 Weissler Dosimetry

Figure 5.4 shows the concentration of produced I_3^- ions vs. amplitude for different frequencies. First and foremost, an essential detail of the graph is that the concentrations for the 24 kHz is not comparable to those with higher frequency due to the significant difference in acoustic power between the Hielscher and Meinhardt ultrasonicators. As seen from this plot, the SD is small for all experiments, which indicates that although the Weissler dosimetry method may not be highly accurate, it is reliable.

For 580 kHz, 860 kHz, and 1140 kHz at 100% amplitude, it is the 860 kHz that gives the highest I_3^- concentration. However, this is not the case for the lower amplitudes. As amplitude (acoustic power) decreases, the results from the higher frequencies tend to become almost inseparable. Moreover, the concentration at 40% is only about 1 µmol/L, and at 20% no sonochemical activity was seen, and consequently not included in the graph. These results comply with the measured acoustic power at both 40% and 20%. Although the ultrasound at 20% amplitude has much higher power, the energy that is dissipated into the liquid (acoustic power) is probably insufficient to exceed the acoustic intensity threshold mentioned in Section 2.1. Hence, no radicals is produced, and reaction 2.11-2.16 cannot occur.

Also, for the Meinhardt experiments the increase in concentration as amplitude increases are in resemblance to the characteristics observed for the acoustic power in Figure 5.2. Such a statement could also be made for the Hielscher (24 kHz) experiments and Figure 5.1. These observations are in correspondence with the expected increase in sonochemical activity with increased acoustic power, which was previously stated in Section 3.

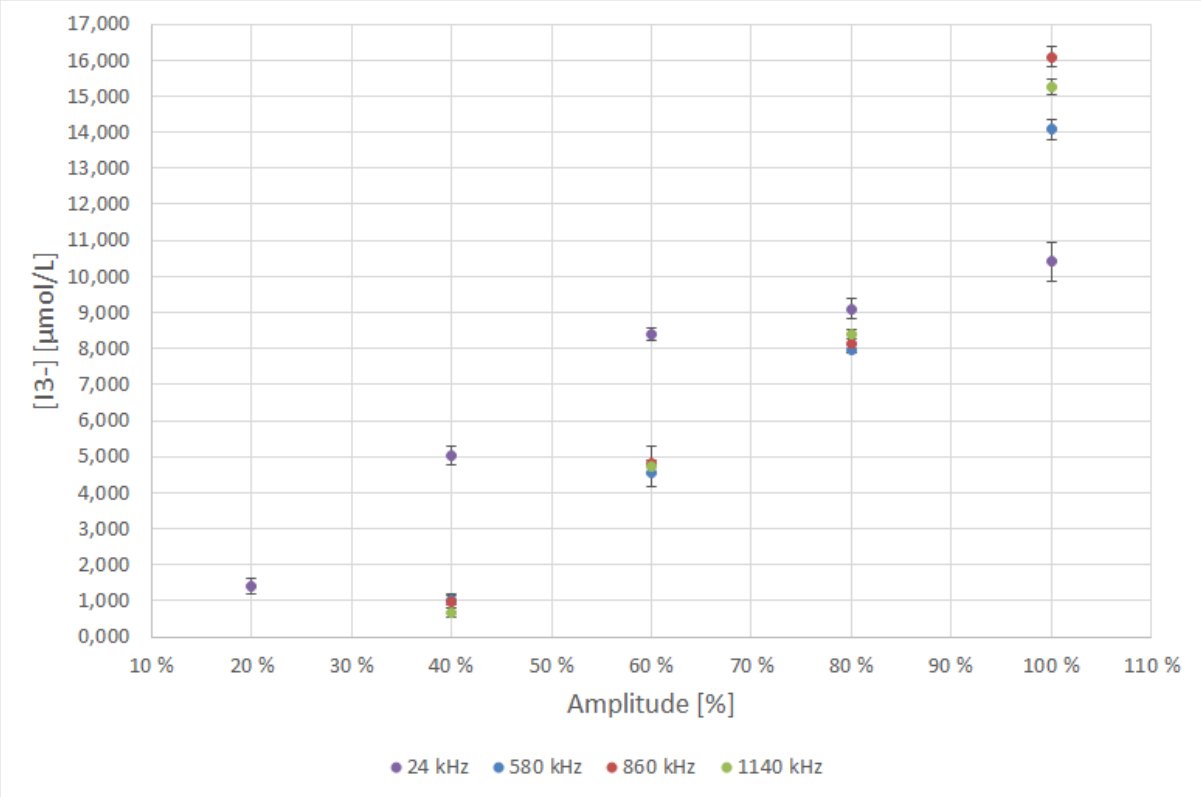

Figure 5.4: Effect of frequency and acoustic power using the Weissler dosimeter ($[I_3^-]$ vs. amplitude). See Appendix, Table A.1 for details about SDs.

By introducing the SE for the results in Figure 5.4, it is possible to compare the 24 kHz results with the higher frequency results. Figure 5.5 presents such SE results for the Weissler dosimeter. Here, the SDs are relatively small, except for those at 40% amplitude at higher frequencies. This is explained by the low acoustic power between 2.7-3.8 W and the way the SE is calculated. As acoustic power increases, the relative variation in SE between the sample selection decrease. To exemplify, the SD for the $[I_3^-]$ at 1140 kHz (Figure 5.4) is greater at 100% amplitude than at 40% amplitude, while the same cannot be said for the SD in Figure 5.5.

The results in Figure 5.5 indicate that the 24 kHz is a much less efficient frequency, compared to the others. The peak SE for 24 kHz is found at around 0.08 µmol/kJ and 60 % amplitude. Overall, the 860 kHz is a slightly more efficient frequency compared to the other frequencies, regardless of amplitude. Note that the results for 860 kHz and 60% amplitude is hidden behind the purple dot in the plot. Furthermore, it is not observed any specific patterns for the higher frequencies in terms of SE vs. amplitude. The SE for 580 kHz, 860 kHz and 1140 kHz both increases and decreases as acoustic power is increased, but generally stays between 0.200 and 0.280 µmol/kJ.

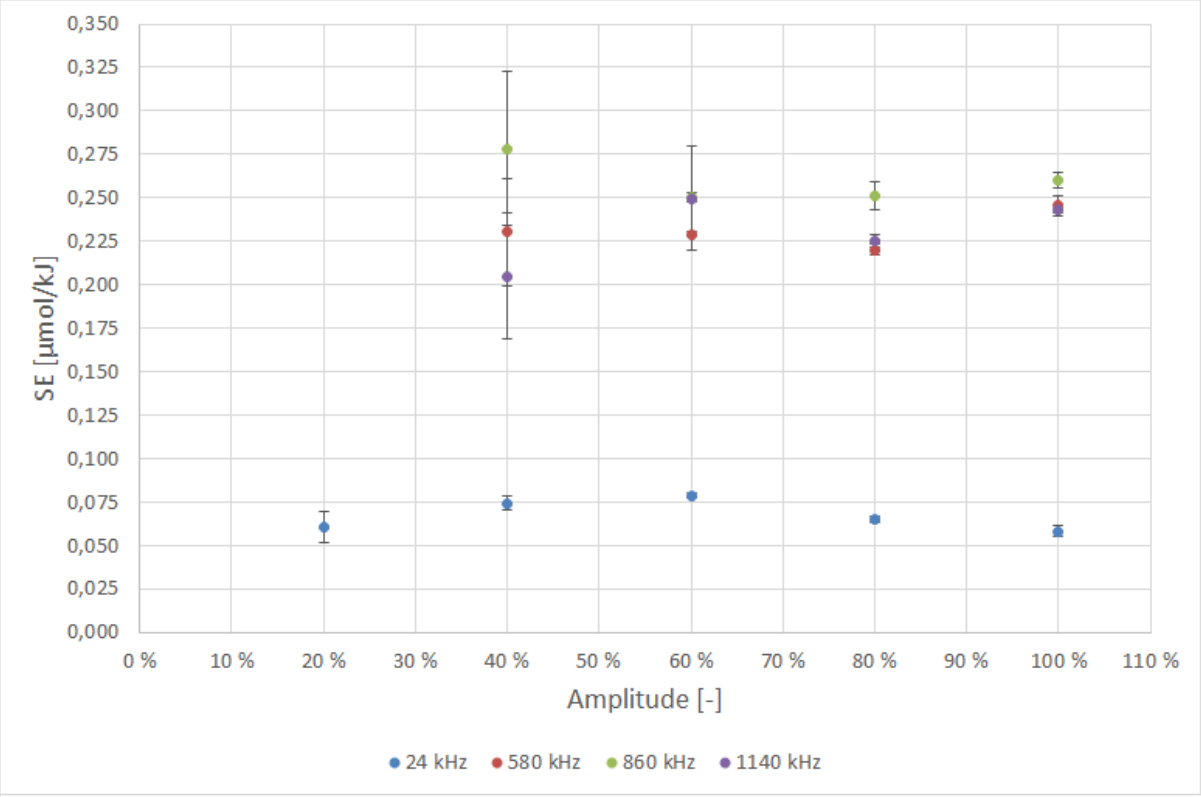

Figure 5.5: Effect of frequency and acoustic power using the Weissler dosimeter (SE vs. amplitude). See Appendix, Table A.1 for details about SDs.

5.3.3 Fricke Dosimetry

Figure 5.6 shows the concentration of produced Fe^{3+} ions vs. amplitude for different frequencies. Like Figure 5.4, the 24 kHz results are not comparable to those with higher frequencies. No sonochemical activity was seen at 20% amplitude for the higher frequencies due to the observed acoustic power of 0 W for the Meinhardt ultrasonicator. Although some small activity was detected at 40% amplitude for the Weissler dosimetry, no Fe^{3+} was observed at this amplitude for the Fricke dosimetry.

The SDs for these experiments are alike for the higher frequencies, but noticeably higher for 24 kHz. Since the Fricke dosimeter also is considered accurate, the inaccuracy is hard to explain. Some cavitation damage observed on the tip of the sonotrode accompanying the Hielscher transducer may be the cause. The cavitation damage appeared during work at higher pressures, which are not associated with this thesis. The damaged sonotrode may have caused unknown changes in the ultrasound. Unfortunately, it was not possible to acquire a new one for this thesis. In spite of this, the damage where only present during the experiments presented in this section.

In Figure 5.6 we can observe similar Fe^{3+} production at 580, 860, and 1140 kHz (for each level of amplitude). This could also be seen for the Weissler experiment. Furthermore the difference between the two dosimeters is considerable, with a maximum $[I_3^-]$ and $[Fe^{3+}]$ of 16.09 µM and 98.32 µM, respectively.

However, the trends also seem to differ for the Fricke and Weissler dosimetry. Whereas the higher frequency results catch up to the 24 kHz results between 80 to 100% amplitude

in terms of $[I_3^-]$ in Figure 5.4, the 24 kHz results dominate at every amplitude for the Fricke dosimetry (Figure 5.6). If the cavitation damage mentioned could be neglected as a reason for this, it can possibly be explained by the fundamental difference between the two dosimetry methods. As mentioned in Section 2.6.1 and 2.6.2, both methods are based on oxidation caused by $OH\cdot$ and H_2O_2. However, Fe^{3+} can also be oxidized by $H\cdot$ and $HO_2\cdot$, which can change the observed sonochemical yield. Although considered to be neglected in sonochemistry, the $H\cdot$ can reduce the amounts of I_2 atoms by reaction 2.17, creating even bigger differences.

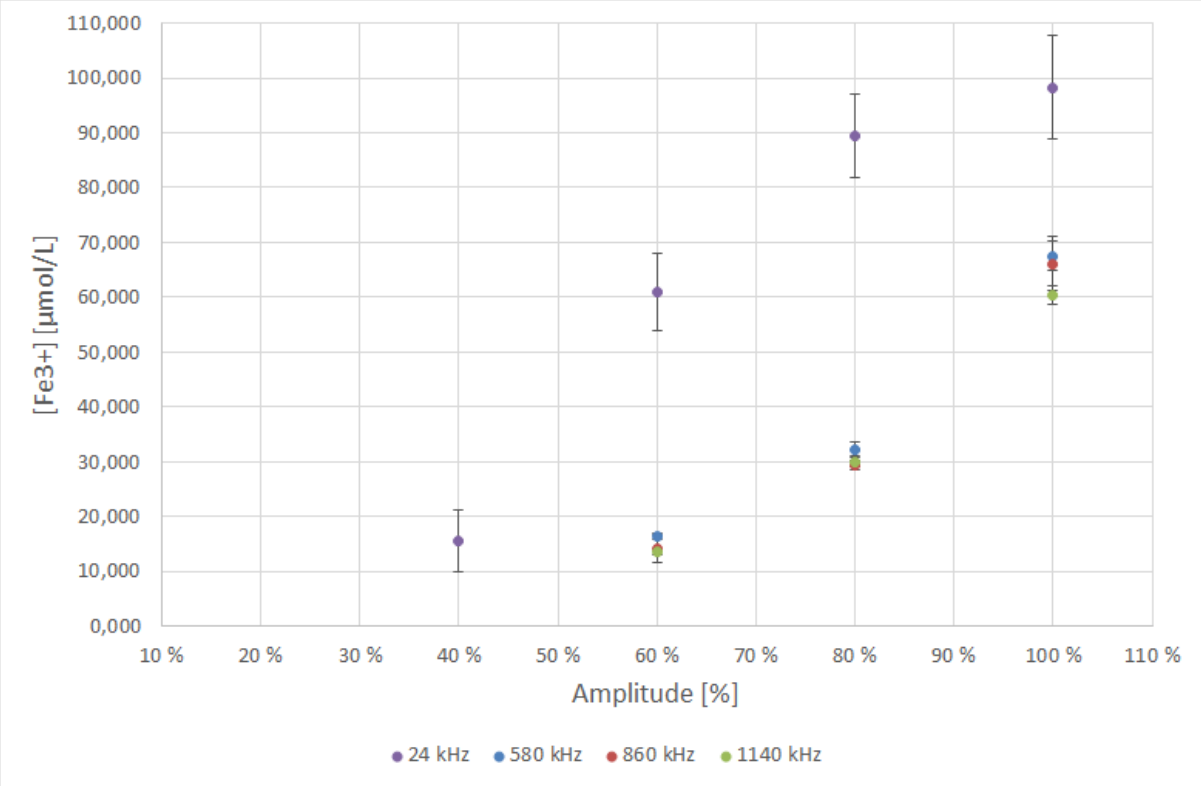

Figure 5.6: Effect of frequency and acoustic power using the Fricke dosimeter ($[Fe^{3+}]$ vs. amplitude). See Appendix, Table A.2 for details about SDs.

The results are also presented in terms of SE in Figure 5.7. From this plot, we can see that the SDs generally are greater than those observed for Figure 5.5 for Weissler dosimetry (except at 40% amplitude). The SE is at its highest at 100% amplitude for 580, 860, and 1140 kHz, and at 80% for the 24 kHz experiments. While the SE increases almost linearly with increased amplitude for the higher frequencies, the 24 kHz results resemble a concave function. As for the effect of frequency, the 580 kHz results provides the overall highest SE, followed by 860, 1140, and 24 kHz. The differences in characteristics and trends for the SE results between the two dosimeters are possibly explained by their difference in oxidising species as mentioned earlier in this section.

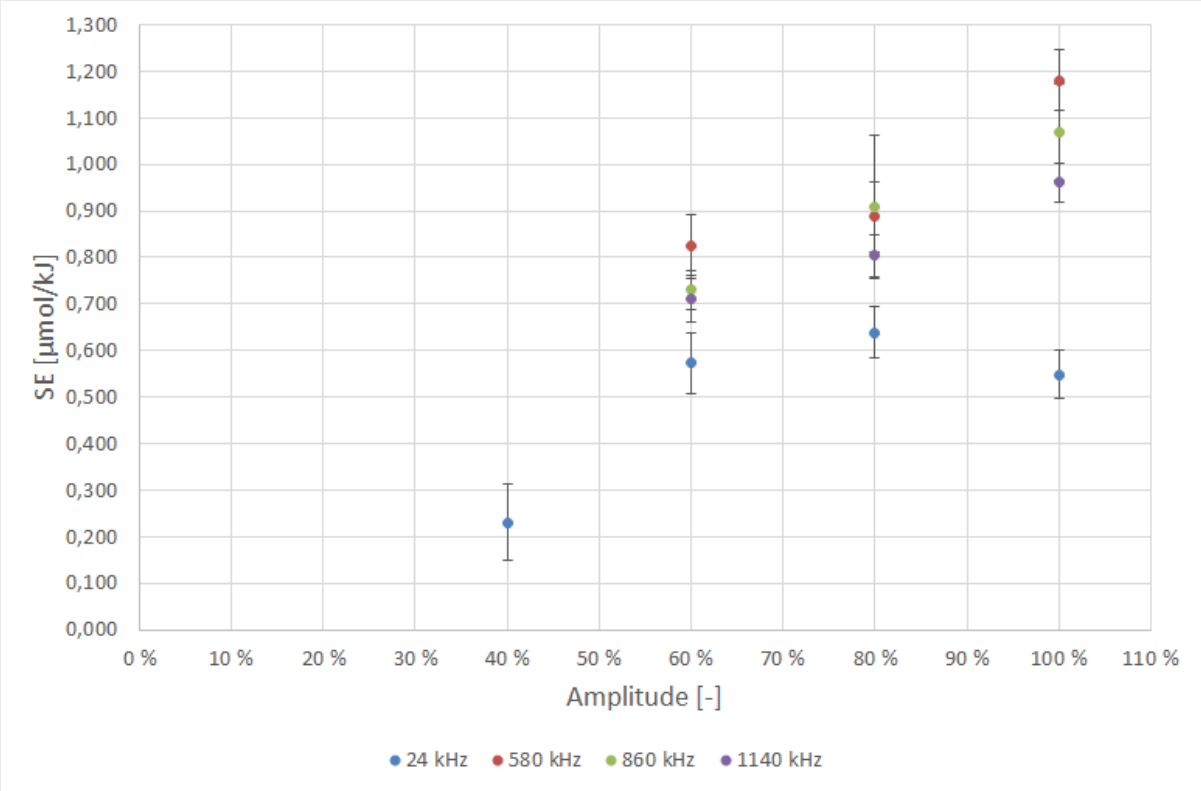

Figure 5.7: Effect of frequency and acoustic power using the Fricke dosimeter (SE vs. amplitude). See Appendix, Table A.2 for details about SDs.

As debated in the Specialization Report [1], the unsonicated zero base samples used for the Weissler dosimetry method remained almost the same with a variation of ±0.0035 in absorbance (A) at $\lambda_{max} = 350$ nm, when deionized water was used as a reference. This graph is found in Appendix A, Figure A.3. However for the work done in this thesis, the zero base samples for the Weissler dosimetry had a variation in absorbance of ±0.015 A, reaching from 0.019 A to 0.049 A. This variation corresponds to a SD of $\sigma = 0.007$ A. As the sample analysis relies upon these zero base samples, it is important to understand why this increase in variation occurs, so that action can be taken to avoid imprecise results. With regard to the previously written Specialization Report, the number of experiments performed was drastically increased for this thesis. Consequently, several different packages of plastic cuvettes were used. These types of cuvettes may be optically different as a result of mass production but are viable for analysis down to 280 nm [45]. Although they are suited for both the Weissler and Fricke dosimeter, the optical difference may explain the variation observed.

Other possible explanations are variations in the solutions, the deionized water, or inaccuracy in the UV-Vis spectrophotometer. As for the prepared solutions, measures were initially taken as discussed in Section 4.3, but some uncertainties like the purity of the compounds remain inevitable. Moreover, the Thermo Scientific Genesys 30 Visible Spectrophotometer, has a reported inaccuracy of ±0.002 A (0-0.3A) and 0.5% (0.301-2.5A). With the considerable variation in zero base absorbance seen for the Weissler dosimetry experiments, an extra measure was taken. For each experiment (both Weissler and Fricke), an unsonicated zero base sample was taken before sonication. In this way, reusing a zero base for several tests are avoided, and variations in the solutions could be neglected.

6 Conclusions

By studying the effect of liquid height, ultrasonic frequency, and acoustic power for the specific sonochemical setup used in this thesis, some indications and trends on sonochemical activity can be emphasized. It is vital to recognize that the results and conclusions in this thesis only apply for this specific sonochemical setup. For the effect of frequency and acoustic power, the SE results are most relevant for comparison of the Hielscher and Meinhardt experiments.

The most distinct trend observed while studying the effect of liquid height was the optimal height at 85.7 mm (250 mL) for 580, 860, and 1140 kHz. These results corresponded and were independent of the dosimetry method. However, differences were seen at 24 kHz with optimal liquid heights of 85.7 mm and 185.1 mm for Fricke and Weissler dosimetry, respectively. Thus, it is inconvenient to make any conclusions for this particular frequency.

For the effect of frequency, which is considered the most important factor for sonochemical activity, some trends can be seen. In terms of sonochemical efficiency, the 24 kHz is less efficient than the higher frequencies. For higher frequencies, SE results are quite similar, and some are impossible to differentiate when the SD is taken into consideration. However, the results indicate that 860 kHz and 580 kHz are slightly more efficient than 1140 kHz. However, higher accuracy is needed in order to make any conclusions.

The effect of acoustic power on sonochemical activity was as expected. As acoustic power increases, the sonochemical activity increases for both Weissler and Fricke dosimetry. Also, the I_3^- production resembled the characteristics of acoustic power measured for the Hielscher and Meinhardt ultrasonicator. In terms of SE for 24 kHz, a peak can be seen at 60% and 80% amplitude for the Weissler and Fricke dosimetry, respectively. For 580 kHz, the SEs remain relatively constant for the Weissler dosimetry, while it increases for Fricke dosimetry. Similar trends can be seen for 860 kHz and 1140 kHz. With different SE patterns for Weissler and Fricke dosimetry, it is inconvenient to make any conclusions for the effect of acoustic power on sonochemical efficiency.

Further Work

One of the factors that impede solid conclusions in the thesis is the dissimilar results obtained from the Weissler and Fricke dosimetry method. Thus, it would be preferable to use a more precise dosimeter such as the terephthalic acid or salicylic acid dosimeter, which both exclusively traps the $OH\cdot$ radicals. Such methods could also possibly reduce the standard deviations seen.

As the experiments were performed at only a few frequencies, amplitudes and liquid heights, more variations of these may give more insight into how these parameters affect radical production. Additionally, potential argon degassing during sonication should be investigated, as it may occur differently under different conditions. Furthermore, more experiments should be done while studying the effect of liquid height in order to determine the reliability and consistency of these results.

References

[1] Lars Martin Ingebrigtsen. "Commissioning a Lab-Scaled Sonochemical Reactor". 2019.

[2] Md Hujjatul Islam, Odne S. Burheim, and Bruno G. Pollet. "Sonochemical and Sonoelectrochemical Production of Hydrogen". In: *Ultrasonics Sonochemistry* 51 (Sept. 2018).

[3] John A. Turner. "Sustainable Hydrogen Production". In: *Science* 305.5686 (2004), pp. 972–974.

[4] Slimane Merouani et al. "Computational engineering study of hydrogen production via ultrasonic cavitation in water". In: *International Journal of Hydrogen Energy* 41.2 (2016), pp. 832–844.

[5] Bruno G. Pollet, ed. *Power Ultrasound in Electrochemistry: From Versatile Laboratory Tool to Engineering Solution*. John Wiley and Sons, Inc., 2012.

[6] Kyuichi Yasui. *Acoustic Cavitation and Bubble Dynamics*. Springer Nature, 2018.

[7] Muthupandian Ashokkumar. "The characterization of acoustic cavitation bubbles – An overview". In: *Ultrasonics Sonochemistry* 18.4 (2011), pp. 864–872.

[8] Muthupandian Ashokkumar and Timothy J. Mason. "Sonochemistry". In: *Kirk-Othmer Encyclopedia of Chemical Technology*. American Cancer Society, 2007.

[9] Timothy G. Leighton. *The Acoustic Bubble*. Academic press, 1994, pp. 531–551.

[10] Kenneth S. Suslick et al. "Acoustic cavitation and its chemical consequences". In: *Philosophical Transactions of the Royal Society of London A: Mathematical, Physical and Engineering Sciences* 357.1751 (1999), pp. 335–353.

[11] Muthupandian Ashokkumar et al. "The detection and control of stable and transient acoustic cavitation bubbles". In: *Physical Chemistry Chemical Physics* 11.43 (2009), pp. 10118–10121.

[12] Yoshiyuki Asakura. "Chapter 5 - Experimental Methods in Sonochemistry". In: *Sonochemistry and the Acoustic Bubble*. Ed. by Franz Grieser et al. Amsterdam: Elsevier, 2015, pp. 119–150.

[13] Giancarlo Cravotto and Pedro Cintas. "Harnessing Mechanochemical Effects with Ultrasound-Induced Reactions". In: *Chemical Science* 3 (Jan. 2012), pp. 295–307.

[14] Slimane Merouani et al. "Sensitivity of free radicals production in acoustically driven bubble to the ultrasonic frequency and nature of dissolved gases". In: *Ultrasonics Sonochemistry* 22 (2015), pp. 41–50.

[15] Elodie Dalodière et al. "Effect of ultrasonic frequency on H2O2 sonochemical formation rate in aqueous nitric acid solutions in the presence of oxygen". In: *Ultrasonics Sonochemistry* 29 (2016), pp. 198–204.

[16] Y. Iida et al. "Sonochemistry and its dosimetry". In: *Microchemical Journal* 80.2 (2005), pp. 159–164.

[17] Ratoarinoro F. Contamine et al. "Power measurement in sonochemistry". In: *Ultrasonics Sonochemistry* 2.1 (1995), S43–S47.

[18] Richard Wood, Judy Lee, and Madeleine Bussemaker. "A parametric review of sonochemistry: Control and augmentation of sonochemical activity in aqueous solutions". In: *Ultrasonics Sonochemistry* 38 (Mar. 2017).

[19] B. Gielen et al. "Characterization of stable and transient cavitation bubbles in a milliflow reactor using a multibubble sonoluminescence quenching technique". In: *Ultrasonics Sonochemistry* 25 (2015), pp. 31–39.

[20] Yoshiyuki Asakura et al. “Effects of ultrasonic frequency and liquid height on sonochemical efficiency of large-scale sonochemical reactors”. In: *Ultrasonics Sonochemistry* 15.3 (2008), pp. 244–250.

[21] Younggyu Son et al. “Liquid Height Effect on Sonochemical Reactions in a 35 kHz Sonoreactor”. In: *Japanese Journal of Applied Physics* 48.7S (2009), 07GM16.

[22] Vijayanand S. Moholkar, Shishir P. Sable, and Aniruddha B. Pandit. “Mapping the cavitation intensity in an ultrasonic bath using the acoustic emission”. In: *AIChE Journal* 46.4 (2000), pp. 684–694.

[23] Parag R. Gogate. “Application of cavitational reactors for water disinfection: current status and path forward”. In: *Journal of environmental management* 85.4 (Dec. 2007), pp. 801–815.

[24] Younggyu Son et al. “Geometric Optimization of Sonoreactors for the Enhancement of Sonochemical Activity”. In: *The Journal of Physical Chemistry C* 115.10 (2011), pp. 4096–4103.

[25] Engineering ToolBox. *Ratios of Specific Heat of Gases*. Accessed 02.04.19. 2003. URL: `https://www.engineeringtoolbox.com/specific-heat-ratio-d_608.html`.

[26] Engineering ToolBox. *Thermal Conductivity of common Materials and Gases*. Accessed 02.04.19. 2003. URL: `https://www.engineeringtoolbox.com/thermal-conductivity-d_429.html`.

[27] Wired Chemist. *Solubilities of Gases in Water at 293 K*. Accessed 02.04.19. 2019. URL: `http://www.wiredchemist.com/chemistry/data/solubilities-gases`.

[28] Slimane Merouani et al. “Influence of experimental parameters on sonochemistry dosimetries: KI oxidation, Fricke reaction and H2O2 production”. In: *Journal of Hazardous Materials* 178.1 (2010), pp. 1007–1014.

[29] Alfred Weissler, Herbert W. Cooper, and Stuart Snyder. “Chemical Effect of Ultrasonic Waves: Oxidation of Potassium Iodide Solution by Carbon Tetrachloride”. In: *Journal of the American Chemical Society* 72.4 (1950), pp. 1769–1775.

[30] Antonio E. Alegria et al. “Sonolysis of aqueous surfactant solutions. Probing the interfacial region of cavitation bubbles by spin trapping”. In: *The Journal of Physical Chemistry* 93 (June 1989).

[31] Carlos Eduardo deAlmeida et al. “A Feasibility Study of Fricke Dosimetry as an Absorbed Dose to Water Standard for 192Ir HDR Sources”. In: *PLOS ONE* 9.12 (Dec. 2014), pp. 1–13.

[32] Dong Chen, Sanjay K. Sharma, and Ackmez Mudhoo. *Handbook on Applications of Ultrasound: Sonochemistry for Sustainability*. CRC Press, 2011, p. 584.

[33] Xingwang Fang, Gertraud Mark, and Clemens von Sonntag. “OH radical formation by ultrasound in aqueous solutions Part I: the chemistry underlying the terephthalate dosimeter”. In: *Ultrasonics Sonochemistry* 3.1 (1996), pp. 57–63.

[34] S. Arrojo, C. Nerín, and Y. Benito. “Application of salicylic acid dosimetry to evaluate hydrodynamic cavitation as an advanced oxidation process”. In: *Ultrasonics Sonochemistry* 14.3 (2007), pp. 343–349.

[35] Gertraud Mark et al. “OH-radical formation by ultrasound in aqueous solution – Part II: Terephthalate and Fricke dosimetry and the influence of various conditions on the sonolytic yield”. In: *Ultrasonics Sonochemistry* 5.2 (1998), pp. 41–52.

[36] Laurent Villeneuve et al. “Assay of hydroxyl radicals generated by focused ultrasound”. In: *Ultrasonics Sonochemistry* 16.3 (2009), pp. 339–344.

[37] Louise Milne, Isobel Stewart, and David H. Bremner. "Comparison of hydroxyl radical formation in aqueous solutions at different ultrasound frequencies and powers using the salicylic acid dosimeter". In: *Ultrasonics Sonochemistry* 20.3 (2013), pp. 984–989.

[38] Kandasamy Thangavadivel et al. "Ultrasound-assisted degradation of methyl orange in a micro reactor". In: *Journal of Environmental Chemical Engineering* 2.3 (2014), pp. 1841–1845.

[39] Tatsuya Torii et al. "Generation and consumption rates of OH radicals in sonochemical reactions". In: *Research on Chemical Intermediates* 30.7 (2004), pp. 713–721.

[40] Manoj Giri et al. "Absorbtion and Fluorescence Spectra of Methyl Orange in Aqueous Solutions". In: *Atti della Fondazione Giorgio Ronchi* 2 (2012).

[41] "Coumarin fluorometry to quantitatively detectable OH radicals in ultrasound aqueous medium". In: *Ultrasonics Sonochemistry* 30 (2016), pp. 18–27.

[42] James G. Speight. "Chapter Five - Sources and Types of Inorganic Pollutants". In: *Environmental Inorganic Chemistry for Engineers*. Ed. by James G. Speight. Butterworth-Heinemann, 2017, pp. 231–282.

[43] AAVOS International. *UV-Vis-spectrometry*. Accessed 23.01.19. 2017. URL: `https://aavos.eu/glossary`.

[44] Michigan State University Department of Chemistry. *UV-Visible Spectroscopy*. Accessed 22.01.19. 2017. URL: `https://www2.chemistry.msu.edu/faculty/reusch/VirtTxtJml/Spectrpy/UV-Vis/uvspec.htm#uv1`.

[45] György Hegyi et al. *Introduction to Practical Biochemistry*. Eötvös Loránd University, 2013. Chap. 4.2. The UV-VIS photometer.

[46] Thermo Fischer Scientific Inc. *Extinction Coefficients: A guide to understanding extinction coefficients, with emphasis on spectrophotometric determination of protein concentration*. Accessed 27.03.19. 2013. URL: `http://tools.thermofisher.com/content/sfs/brochures/TR0006-Extinction-coefficients.pdf`.

[47] Myer Kutz, ed. *Handbook of Measurement in Science and Engineering*. Vol. 3. John Wiley and Sons, Inc., 2016. Chap. Fluorescence Spectroscopy.

[48] PerkinElmer Inc. *An Introduction to Fluorescence Spectroscopy*. Accessed 24.01.19. 2000. URL: `https://www.chem.uci.edu/~dmitryf/manuals/Fundamentals/Fluorescence%20Spectroscopy.pdf`.

[49] M.V. Moreno-Arribas and M.C. Polo. "CHROMATOGRAPHY | High-performance Liquid Chromatography". In: *Encyclopedia of Food Sciences and Nutrition (Second Edition)*. Ed. by Benjamin Caballero. Second Edition. Oxford: Academic Press, 2003, pp. 1274–1280.

[50] Seneca. "CHAPTER 2 - Alkaloid Chemistry". In: *Alkaloids - Secrets of Life*. Ed. by Tadeusz Aniszewski. Amsterdam: Elsevier, 2007, pp. 61–139.

[51] University of Antioquia - Instituto de Química. *Basic Principles of HPLC*. Accessed 25.01.19. URL: `http://quimica.udea.edu.co/~carlopez/cromatohplc/hplc_e.pdf`.

[52] Frank P. Incropera et al. *Principles of Heat and Mass Transfer*. 7th edition. John Wiley Sons Singapore Pte. Ltd., 2013, p. 8.

[53] L. Hallez et al. "Characterization of HIFU transducers designed for sonochemistry application: Acoustic streaming". In: *Ultrasonics Sonochemistry* 29 (2016), pp. 420–427.

Appendix A Tables and Figures

Table A.1: Standard deviations for I_3^- concentration and SE

f [kHz]	A [%]	$\sigma_{[I_3^-]}$	σ_{SE}
24	100	0.539	0.003
24	80	0.278	0.002
24	60	0.160	0.002
24	40	0.262	0.004
24	20	0.212	0.009
580	100	0.277	0.005
580	80	0.111	0.003
580	60	0.022	0.001
580	40	0.139	0.031
860	100	0.273	0.004
860	80	0.273	0.008
860	60	0.059	0.003
860	40	0.155	0.044
1140	100	0.219	0.003
1140	80	0.135	0.004
1140	60	0.567	0.030
1140	40	0.118	0.036

Table A.2: Standard deviations for Fe^{3+} concentration and SE

f [kHz]	A [%]	$\sigma_{[Fe^{3+}]}$	σ_{SE}
24	100	9.56	0.053
24	80	7.58	0.054
24	60	7.07	0.066
24	40	5.62	0.083
580	100	3.79	0.066
580	80	2.74	0.076
580	60	1.37	0.069
860	100	6.44	0.104
860	80	5.01	0.155
860	60	0.79	0.041
1140	100	2.59	0.041
1140	80	1.64	0.044
1140	60	0.95	0.050

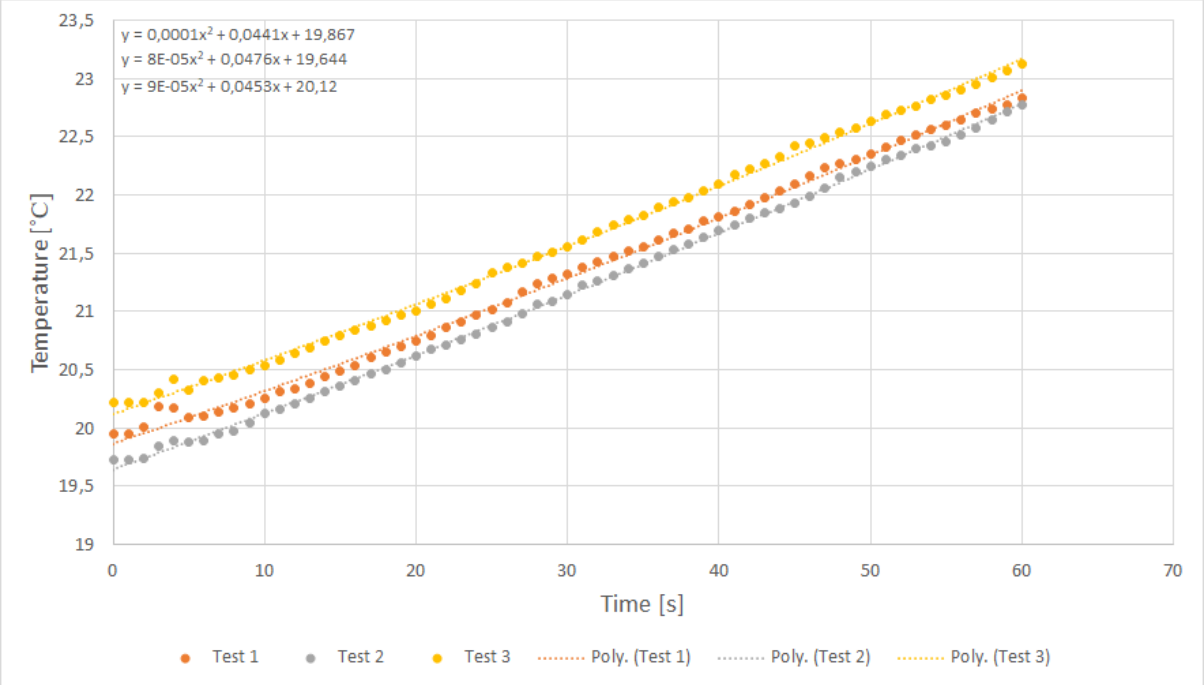

Figure A.1: Example of second order polynomial curve fitting used in calorimetry. This specific plot is taken from three calorimetric experiments at 250 mL for 580 kHz.

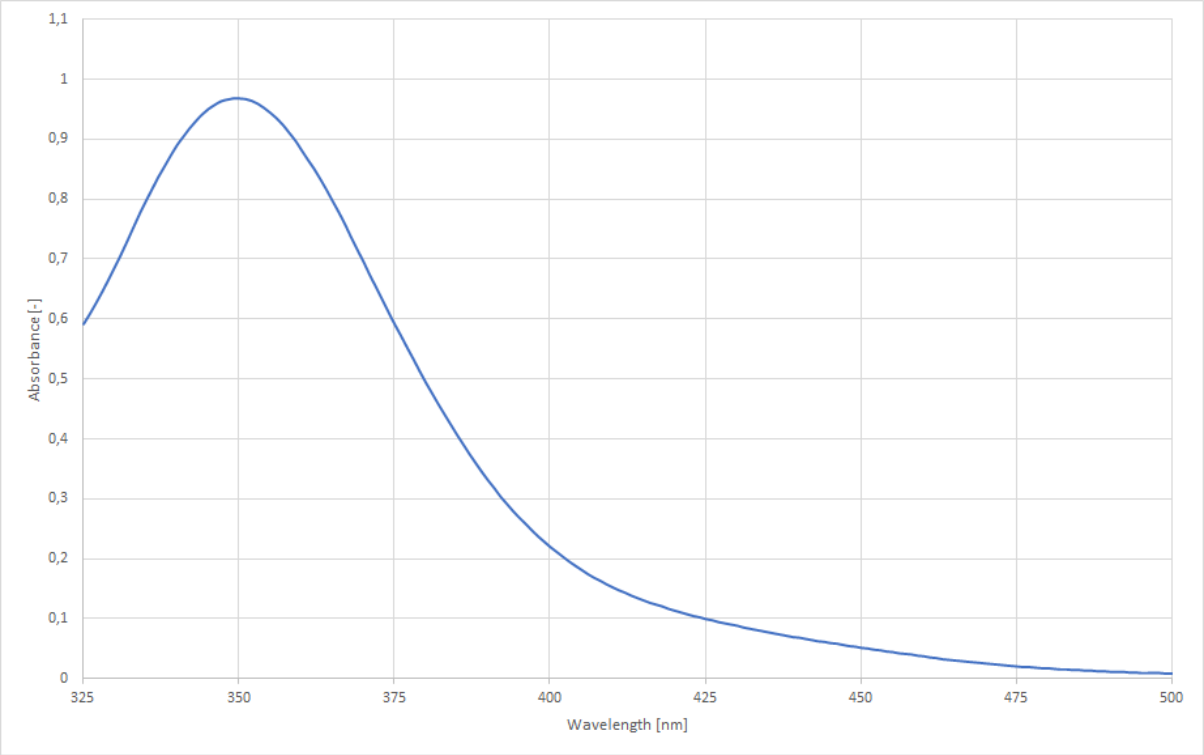

Figure A.2: A typical absorbance scan using Weissler dosimetry ($\lambda_{max} = 350$ nm)

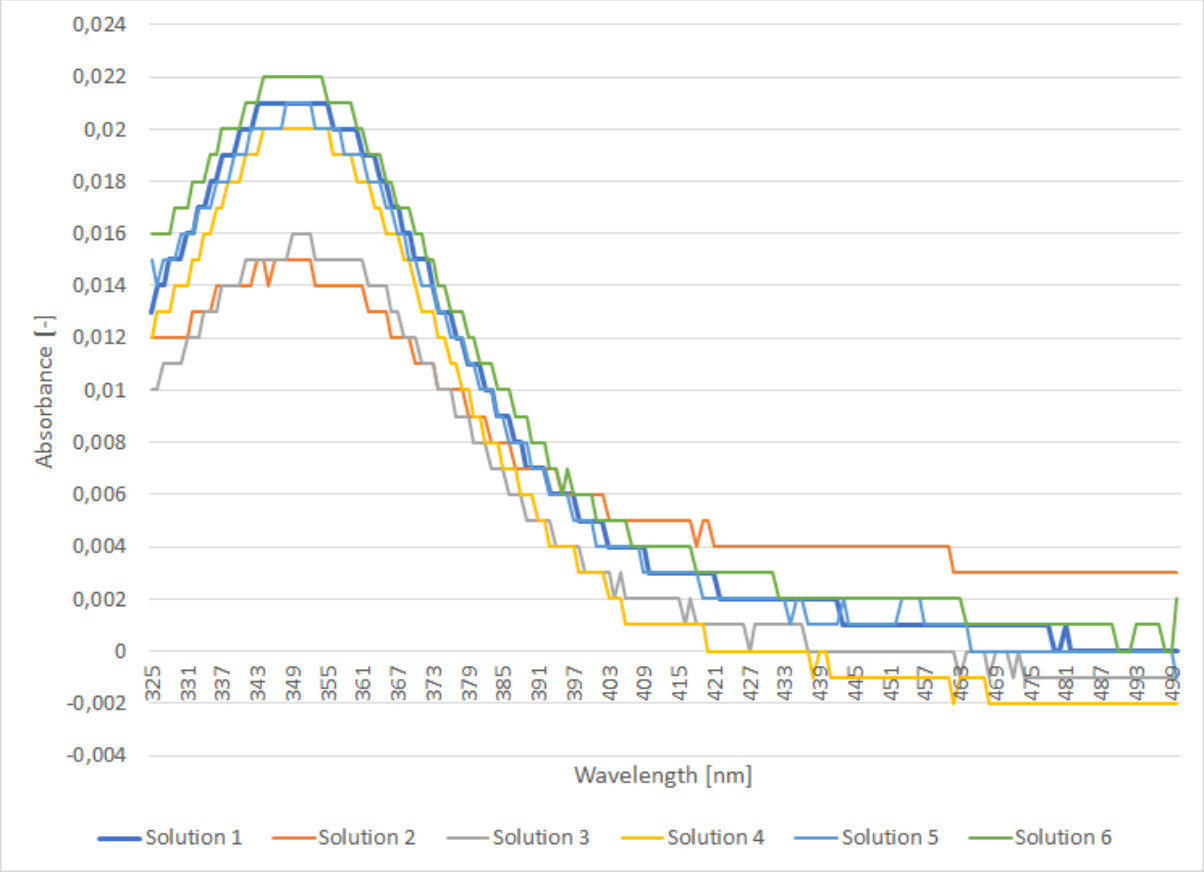

Figure A.3: Absorption scans of six unsonicated 0.1M KI solutions with deionized water as zero base. Variation of ±0.0035 in absorbance at 350 nm. The notches in the graph is due to the spectrometers resolution limit [1].

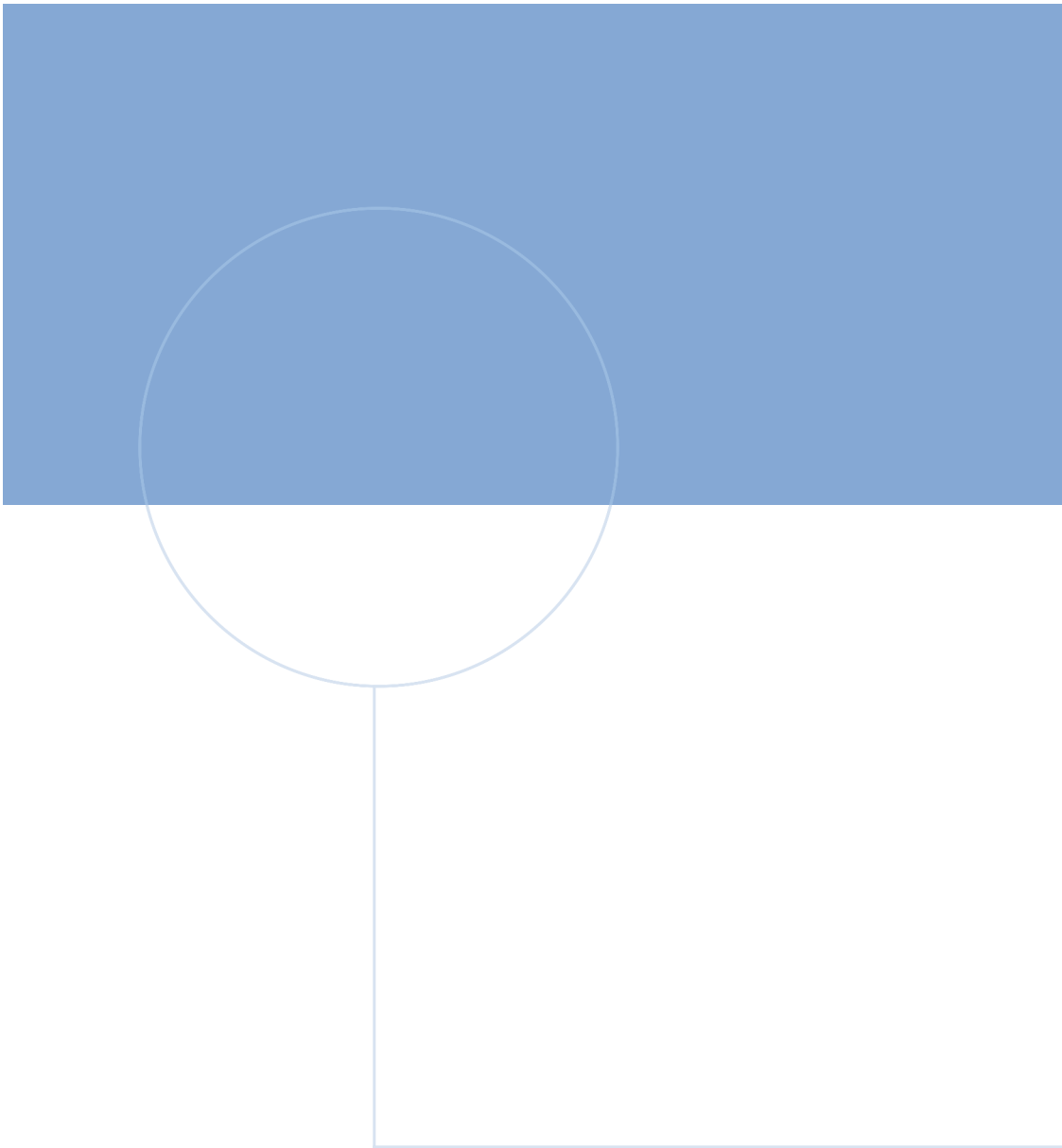

NTNU
Norwegian University of
Science and Technology